

AD-A143 820

OPTICAL AND ELECTRICAL CHARACTERIZATION OF MULTIPLY
DOPED SILICON: A STUD. (U) DAYTON UNIV OH RESEARCH INST
G J BROWN ET AL FEB 84 AFWAL-TR-83-4108

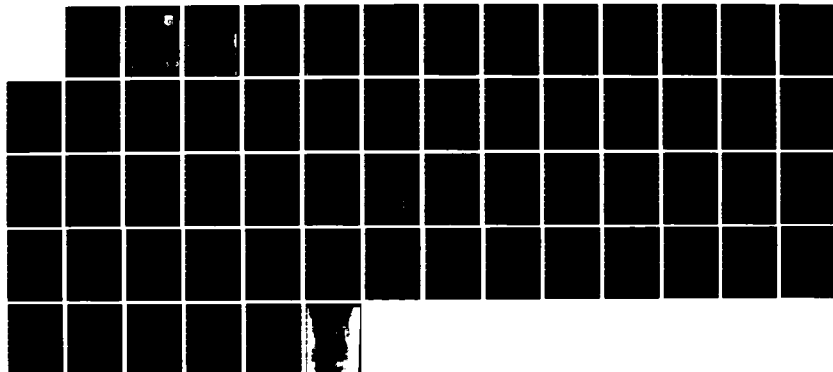
1/1

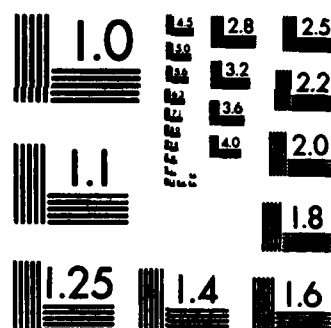
UNCLASSIFIED

F33615-81-C-5095

F/G 20/12

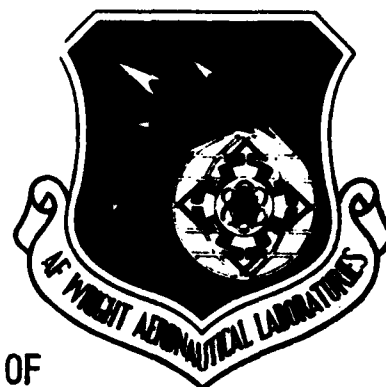
NL





MICROCOPY RESOLUTION TEST CHART
NATIONAL BUREAU OF STANDARDS-1963-A

12



OPTICAL AND ELECTRICAL CHARACTERIZATION OF
MULTIPLY DOPED SILICON: A STUDY OF THE
Si:(In, Al) SYSTEM

Gail J. Brown
Melvin C. Ohmer
David W. Fischer
John J. Rome
Ken D. Beasley
Patrick M. Hemenger

Laser and Optical Materials Branch
Electromagnetic Materials Division

David H. Brown
University of Dayton Research Institute
Dayton, Ohio 45469

February 1984

Interim Report for Period March 1981 - March 1983

Approved for public release; distribution unlimited.

AD-A143 820

DTIC FILE COPY

MATERIALS LABORATORY
AIR FORCE WRIGHT AERONAUTICAL LABORATORIES
AIR FORCE SYSTEMS COMMAND
WRIGHT-PATTERSON AIR FORCE BASE, OHIO 45433

DTIC
ELECTE
AUG 1 1984
S A B

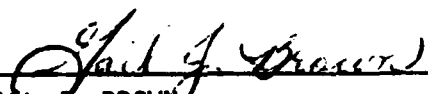
84 07 31 088


NOTICE

When Government drawings, specifications, or other data are used for any purpose other than in connection with a definitely related Government procurement operation, the United States Government thereby incurs no responsibility nor any obligation whatsoever; and the fact that the government may have formulated, furnished, or in any way supplied the said drawings, specifications, or other data, is not to be regarded by implication or otherwise as in any manner licensing the holder or any other person or corporation, or conveying any rights or permission to manufacture use, or sell any patented invention that may in any way be related thereto.

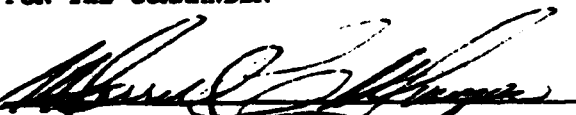
This report has been reviewed by the Office of Public Affairs (ASD/PA) and is releasable to the National Technical Information Service (NTIS). At NTIS, it will be available to the general public, including foreign nations.

This technical report has been reviewed and is approved for publication.


GAIL J. BROWN
Project Monitor
Laser & Optical Materials Branch


G. EDWARD KUHL, Chief
Laser & Optical Materials Branch
Electromagnetic Materials Division

FOR THE COMMANDER


MERRILL L. MINGES, Chief
Electromagnetic Materials Division
Materials Laboratory
Air Force Wright Aeronautical Laboratories

"If your address has changed, if you wish to be removed from our mailing list, or if the addressee is no longer employed by your organization please notify AFWAL/MLPO, W-PAFB, OH 45433 to help us maintain a current mailing list".

Copies of this report should not be returned unless return is required by security considerations, contractual obligations, or notice on a specific document.

UNCLASSIFIED

SECURITY CLASSIFICATION OF THIS PAGE (When Data Entered)

REPORT DOCUMENTATION PAGE		READ INSTRUCTIONS BEFORE COMPLETING FORM
1. REPORT NUMBER AFJAL-TR-83-4108	2. GOVT ACCESSION NO. A143820	3. RECIPIENT'S CATALOG NUMBER
4. TITLE (and Subtitle) OPTICAL AND ELECTRICAL CHARACTERIZATION OF MULTIPLY DOPED SILICON: A STUDY OF THE Si:(In, Al) SYSTEM		5. TYPE OF REPORT & PERIOD COVERED Interim Technical Report Mar 1981-Mar 1983
7. AUTHOR(s) Gail J. Brown, Melvin C. Ohmer, David W. Fischer, John J. Rome, Ken D. Seasley, Patrick M. Hemenger AFJAL/MLPO and David H. Brown, Univ of Dayton		6. PERFORMING ORG. REPORT NUMBER
9. PERFORMING ORGANIZATION NAME AND ADDRESS Materials Laboratory (AFJAL/MLPO) Air Force Wright Aeronautical Laboratories (AFSC) Wright-Patterson Air Force Base, Ohio 45433		8. CONTRACT OR GRANT NUMBER(s) F30615-81-C-5095 in part
11. CONTROLLING OFFICE NAME AND ADDRESS Materials Laboratory (AFJAL/MLPO) Air Force Wright Aeronautical Laboratories (AFSC) Wright-Patterson Air Force Base, Ohio 45433		10. PROGRAM ELEMENT, PROJECT, TASK AREA & WORK UNIT NUMBERS Program Element 61102F Project 2305 Task 2006Q1 Work Unit 2306Q106
14. MONITORING AGENCY NAME & ADDRESS (if different from Controlling Office)		12. REPORT DATE February 1984
		13. NUMBER OF PAGES 59
		15. SECURITY CLASS. (of this report) Unclassified
		15a. DECLASSIFICATION/DOWNGRADING SCHEDULE
16. DISTRIBUTION STATEMENT (of this Report) Approved for public release; distribution unlimited.		
17. DISTRIBUTION STATEMENT (of the abstract entered in Block 20, if different from Report)		
18. SUPPLEMENTARY NOTES		
19. KEY WORDS (Continue on reverse side if necessary and identify by block number) Silicon, aluminum, indium, acceptors, absorption spectra, excitation spectra, x-levels, photothermal ionization, Hall effect, photoluminescence, photoconductivity, carbon, oxygen.		
20. ABSTRACT (Continue on reverse side if necessary and identify by block number) Infrared absorption, spectral photoconductivity, photoluminescence, and Hall effect transport measurements have been used to study the optical and electrical properties of silicon single crystals grown by the Czochralski method, which were intentionally doped with indium and aluminum. Thermal annealing did not produce the expected concentrations of In-X acceptors but did increase the concentration of donors in this material. The Al-X level was observed in a concentration of 1% of the parent concentration. Temperature		

UNCLASSIFIED

SECURITY CLASSIFICATION OF THIS PAGE(When Data Entered)

20. ABSTRACT - Continued

dependence of the intensity of Al-X excited states was determined by photothermal ionization and observed to be the same as that of simple Group IIIA acceptors. In photothermal ionization spectra the indium and aluminum excited state lines remain as negative peaks up to higher sample temperatures than observed in singly doped samples. Oxygen and carbon were observed via background subtraction in the photoconductivity spectra. In photoconductivity and absorption typically only the four most tightly bound excited states were observed. Concentrations of dopants and impurities determined by Hall effect and absorption differed substantially for these multiply-doped samples. Photoluminescence showed no evidence of Al bound exciton radiative recombination, consistent with an exciton tunneling mechanism, and, contrary to previous studies of FZ Si: (In, Al), no isoelectronic luminescence was observed. The addition of aluminum to Si:In did not produce In-X.

UNCLASSIFIED

SECURITY CLASSIFICATION OF THIS PAGE(When Data Entered)

FOREWORD

This report describes the results of a systematic study of the electrical and optical properties of Czochralski (CZ) grown silicon crystals intentionally doped with indium and aluminum. The work was performed under two work units of Basic Research Task 2306Q1. Inhouse studies conducted by personnel of the Laser and Optical Materials Branch, Electromagnetic Materials Division, Materials Laboratory, Air Force Wright Aeronautical Laboratories, Wright-Patterson Air Force Base, Ohio 45433 under Project No. 2306, Task No. 2306Q1, Work Unit 2306Q106 provided the results of Hall effect, infrared absorption and photoconductivity measurements. The results of photoluminescence measurements were provided by studies conducted by personnel of the University of Dayton Research Institute, Dayton, Ohio 45469 under Contract No. F33615-81-C-5095, Work Unit 2306Q111. The report covers work performed during the period March 1981 through March 1983. The multiple doped silicon crystals investigated were grown under Contract No. F33615-80-C-5026 by the Honeywell Corporate Technology Center.

Accession For	
NTIS GFA&I	<input checked="checked" type="checkbox"/>
DTIC TAB	<input type="checkbox"/>
Unannounced	<input type="checkbox"/>
Justification	
By	
Distribution/	
Availability Codes	
Dist	Avail and/or Special
A-1	



TABLE OF CONTENTS

SECTION	PAGE
I INTRODUCTION	1
II ABSORPTION MEASUREMENTS	7
III PHOTOCONDUCTIVITY MEASUREMENTS	16
IV PHOTOLUMINESCENCE MEASUREMENTS	23
V HALL EFFECT MEASUREMENTS	25
VI CONCLUSIONS AND RECOMMENDATIONS	38
APPENDIX A SAMPLE LISTING AND WAFER CUTTING DIAGRAM	43
APPENDIX B CARBON AND OXYGEN LOCAL MODE ABSORPTION IN PHOTOCONDUCTIVITY	44
REFERENCES	48

LIST OF ILLUSTRATIONS

FIGURE		PAGE
1	Simplified Energy Level Diagram For An Indium Doped Silicon Extrinsic Detector	2
2	X-Center Line Energy vs. Mean Energy For Acceptor Pairs In Si And Ge	4
3	X-Level Concentration Anneal Dependence For Float-Zoned And Czochralski Grown Si:In	6
4	Infrared Absorption Spectra Of As-Grown Si:(In, Al) Samples 0797 And 0798	8
5	Infrared Absorption Spectrum Of Sample 0798 Showing The Indium $P_{3/2}$ Excitation Lines And The Oxygen Local Mode Absorption	11
6	Infrared Absorption Spectrum Of Sample 0798 Showing Boron And Aluminum-X $P_{3/2}$ Excitation Lines	12
7	Infrared Absorption Spectra Of Sample 0797 Before And After Annealing	15
8	Photoconductivity And Infrared Absorption Spectra For As-Grown CZ Si:(In, Al)	17
9	Temperture Dependence Of The Photothermal Ionization Of The Aluminum X-Level Line 4	19
10	Aluminum X-Level Line 4 Intensity vs. Reciprocal Temperature	20
11	Photoconductivity Spectra Of Sample 0799' Before And After Annealing	22
12	Photoluminescence Of As-Grown CZ Si:(In, Al) Showing Indium Bound-Exciton Features	24
13	Hole Concentration vs. $1000/T$ For (Δ) As-Grown CZ Si:(In, Al), (\diamond) Annealed CZ, And FZ Si:(In, Al) Samples	30
14	Hall Mobility vs. Temperature For (Δ) As-Grown CZ Si:(In, Al), (\diamond) Annealed CZ, And FZ Si:(In, Al) Samples	31
15	Hall Mobility vs. $1000/T$ For (Δ) As-Grown CZ Si:(In, Al), (\diamond) Annealed CZ, And FZ Si:(In, Al) Samples	32

LIST OF ILLUSTRATIONS (Concluded)

FIGURE		PAGE
16	Hall Coefficient vs. $1000/T$ For (Δ) As-Grown CZ Si:(In, Al), (\diamond) Annealed CZ, And FZ Si:(In, Al) Samples	33
17	Resistivity vs. $1000/T$ For (Δ) As-Grown CZ Si:(In, Al), (\diamond) Annealed CZ, And FZ Si:(In, Al) Samples	34
18	Hole Concentration vs. $1000/T$ For Sample 0795-I: (Y) As Grown, (O) After First Anneal, (Δ) Second Run After First Anneal, (\diamond) After Second Anneal, And (+) Thinned Sample	36
19	Location Of Crack On Thinned van der Pauw Sample 0795-I	37
20	Spectral Representation Of Group IIIA Acceptor Energies In Silicon	41
A-1	Sample Listing And Wafer Cutting Diagram	43
B-1	Carbon Local Mode Absorption Peak In Photoconductivity Spectrum Of CZ Si:(In, Al)	45
B-2	Oxygen Local Mode Absorption Peaks in Photoconductivity Spectrum Of CZ Si:(In, Al)	46
B-3	Sample Temperature vs. Ratio of $1128\text{cm}^{-1}/1136\text{cm}^{-1}$ Oxygen Peak Heights	47

LIST OF TABLES

TABLE		PAGE
1	Acceptor Ionization Energies of Group IIIA Elements And Their Related X-Levels In Silicon	2
2	Impurity Concentrations Determined By IR Absorption For CZ Si:(In, Al) Samples	9
3	Calibration Factors Used To Determine Concentrations By IR Absorption	10
4	Hall Effect Concentration Values For As-Grown CZ Si:(In, Al)	27
5	Hall Effect Concentration Values For Samples 0795-I, As-Grown And Post-Anneal	28
6	Hall Effect Concentration Values For Sample 0795-I Before And After Polishing To Thin The Sample	35
7	Diffusion Coefficients In Silicon	39
8	Impurity Concentrations Determined By Absorption And Hall Measurements For As-Grown CZ Si:(In, Al) Samples	41

SECTION I

INTRODUCTION

The Air Force and other DOD departments and agencies have long supported the development of technologies required to produce high resolution infrared imaging systems with superior range capability. Extrinsic silicon infrared detector materials technology may be utilized in those systems which require a large number of detectors with identical photo-response because it is compatible with conventional charge-coupled device (CCD) signal processing, dopant and impurity uniformity is inherently superior to compound semiconductors, and the overall technology is of potentially lower cost.

The properties of Si doped with Group IIIA elements boron, aluminum, gallium, indium, and thallium are fairly well understood and are quite important to extrinsic detector technology. A simplified energy level diagram for an indium doped (extrinsic) silicon detector is shown in Figure 1. This detector operates in a photoconductive mode. A dopant, in this case In, which has an infrared response in the desired spectral region is first introduced. In this p-type detector infrared photons excite holes from the In level into the valence band which is observed as a change in the resistivity of the material. The dopants In and Tl are useful for detection in the 3-5 micron atmospheric window while Ga is the leading candidate for the 8-14 micron atmospheric window. The long-wavelength cut-off for these dopants is given in Table 1.

Presently, boron and aluminum are residual impurities even in the highest purity silicon currently manufactured. Gallium and aluminum have similar ionization energies and both have potential applications in space systems for infrared detection in the 8-17 micron region. However, Al suffers in comparison to Ga in this context due to its proclivity for complexing with oxygen (Reference 1). As a rule of thumb, a dopant with the shortest out-off wavelength compatible with the spectral range required should be selected for optimum, i.e. highest, operating temperature to minimize the refrigeration requirement. Also, the concentration of levels shallower than the dopant level should be minimized and then uniformly

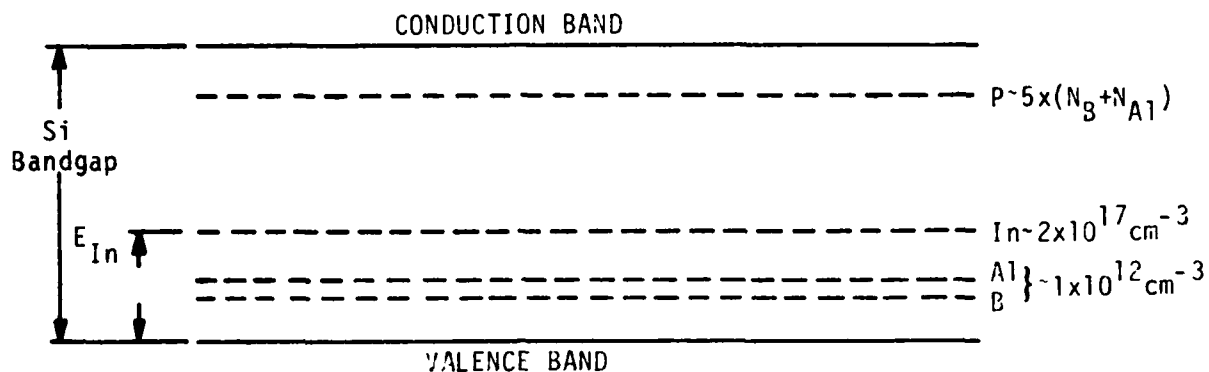


Figure 1. Simplified Energy Level Diagram For An Indium Doped Silicon Extrinsic Detector

TABLE 1

ACCEPTOR IONIZATION ENERGIES OF GROUP IIIA
ELEMENTS AND THEIR RELATED X-LEVELS IN SILICON

Dopant	Energy Level	Cut-off Wavelength	Energy of Associated x-Level
B	.044	27.6 μm	.037
Al	.069	18.5 μm	.056
Ga	.073	17.2 μm	.057
In	.156	7.9 μm	.113
Tl	.246	5.0 μm	.18

overcompensated for uniform large photoresponse (uniform large majority carrier lifetime). For 300K black-body backgrounds, the operating temperatures for Si:Tl, Si:In, and Si:Ga are respectively 90K, 60K, and 25K for background limited (BLIP) performance. These BLIP temperatures are obtained by eliminating generation-recombination (GR) noise due to shallower levels by counterdoping, usually with phosphorus. This moves the Fermi level well above the shallow impurity levels.

In the late 1970's, the Defense Advanced Research Projects Agency (DARPA) sponsored the High Altitude Large Optics (HALO) program which attempted to develop monolithic two-dimensional Si:In detector arrays. As a result of this program a surprising discovery was reported (Reference 2) in 1977: an x-level related to In was observed in Si:In in concentrations greater than 100 times the residual boron and aluminum concentrations and with an acceptor ionization energy about 70% of that for In. Uncompensated, this x-level reduced T_{blip} for Si:In from 60K to 40K, an unacceptable temperature penalty. Because of its high concentration, compensation of the x-level could result in unacceptably low and non-uniform photoresponse in the Si:In detectors. Research programs were then initiated to identify and eliminate this x-level from Si:In which subsequently led to the discovery that x-levels were associated with all Group IIIA acceptors in Si. The ionization energies for these levels are listed in Table 1.

A plausible model for x-levels is an acceptor-carbon next nearest neighbor pair (References 3,4,5) which suggests that a practical solution to the x-level problem is to reduce the carbon concentration in Si to as low a value as possible. However, an empirical rule (Reference 5) for calculating the ionization energy of x-level acceptors as the mean energy of two appropriate Group IIIA acceptors in Si and Ge was discovered which seemed to imply that x-levels result from interactions between substitutional Group IIIA acceptors. The agreement between observed and calculated values of x-level ionization energies is illustrated in Figure 2. In the case of the indium-related x-level an In and Al pair (Reference 5) was indicated, providing a motivation for studying silicon crystals intentionally doped with In and Al. In this case the role of carbon in the formation of a molecular x-level might be that of a catalyst or

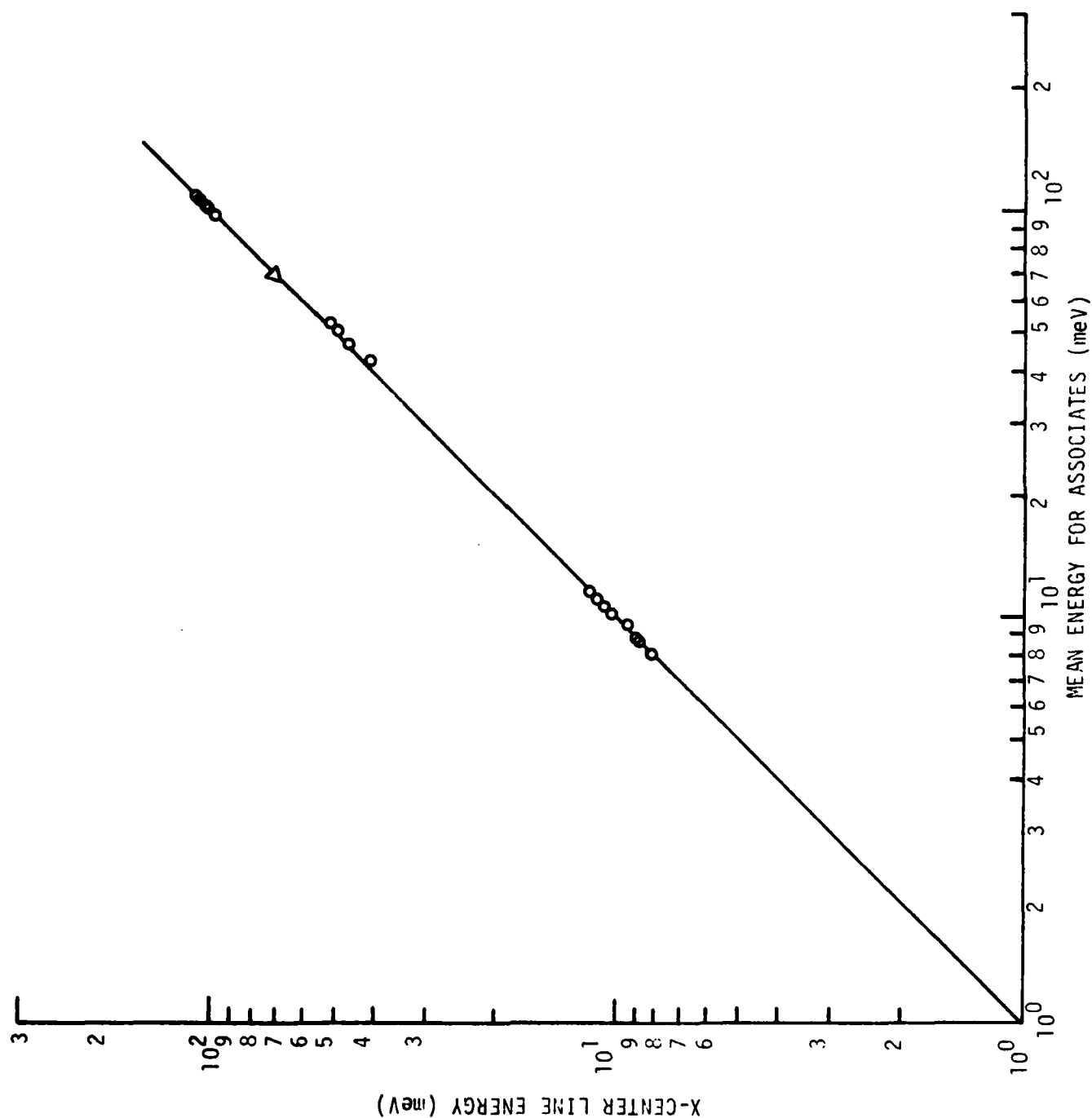


Figure 2. X-Center Line Energy vs. Mean Energy For Acceptor Pairs In Si And Ge

stabilizer. For example, the diffusion of phosphorus in carbon doped silicon is enhanced by a strain mechanism (Reference 6).

Because of the uncertainty surrounding the involvement of Al in indium x-level formation, a program was initiated to investigate the formation of x-levels in silicon crystals grown by float-zone (FZ) and Czochralski (CZ) methods and intentionally doped with indium and aluminum. The results of the first task on FZ Si:(In,Al) have been previously reported (Reference 7). The results of the second task on Si:(In,Al) grown by the CZ method are the subject of this report.

The stability of x-levels is quite different in crystals grown by the two techniques as shown in Figure 3 which provides data taken by Hughes Research Laboratories (Reference 8). Concentrations of x-levels in CZ Si crystals can be easily changed in a well-defined and reversible way by thermal annealing while in FZ crystals such control is not possible. CZ Si often contains 10-1000 times the concentration of oxygen compared to FZ Si; oxygen may therefore play a role in the formation of x-levels in Si and a study of x-levels in co-doped crystals would have been incomplete had this effect not been investigated.

In the following sections, the results of low temperature infrared absorption, spectral photoconductivity, infrared photoluminescence, and temperature-dependent Hall effect measurements on CZ Si:(In,Al) are reported and discussed. The data were obtained on as-grown samples and on samples annealed for one-half hour at 650° followed by four hours at 600°C in an argon ambient. This two step anneal was selected to reduce oxygen related donor concentrations and establish a state of thermal equilibrium between x-level concentrations and major dopant concentrations in accord with Figure 3.

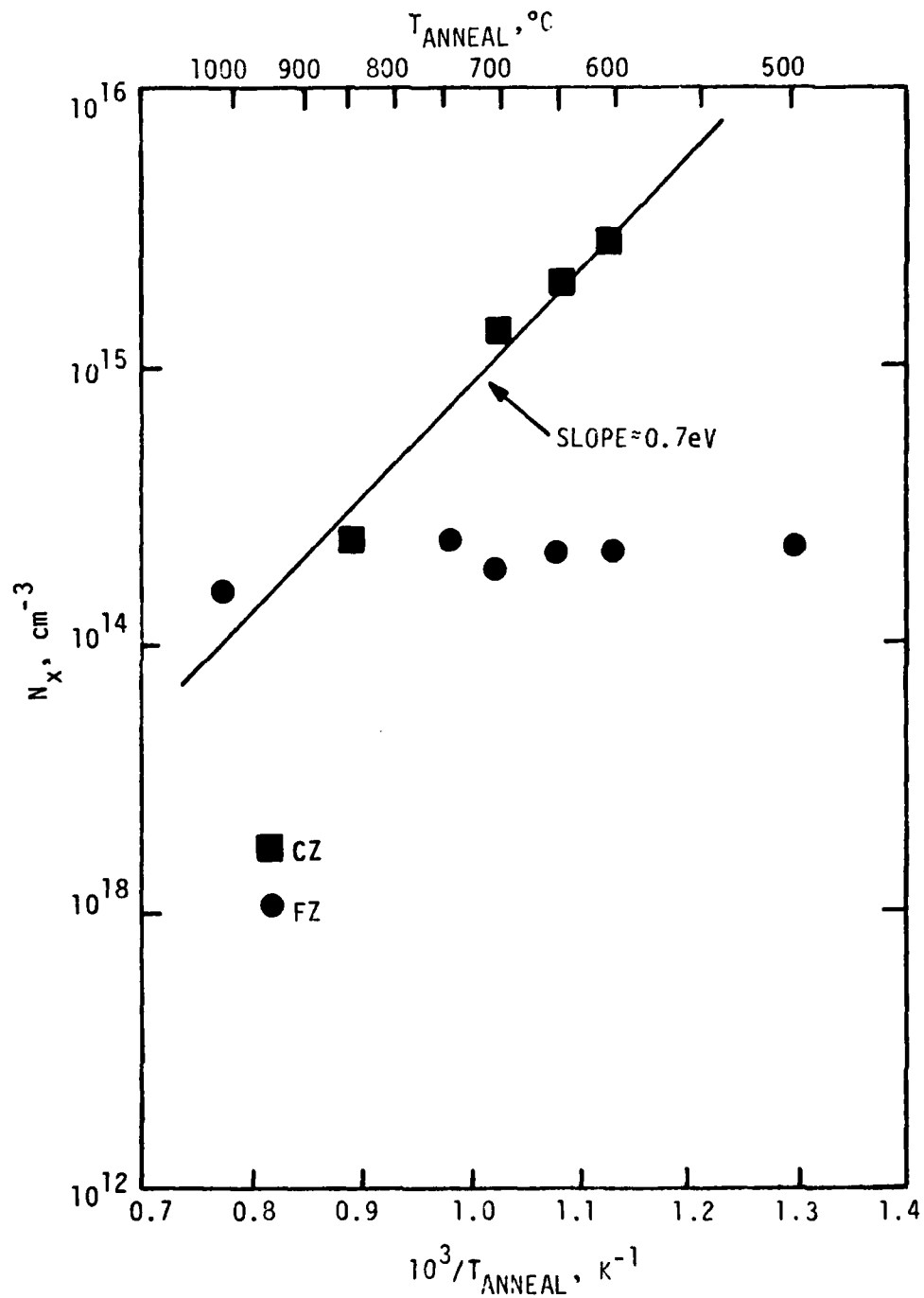


Figure 3. X-Level Concentration Anneal Dependence For Float-Zoned And Czochralski Grown Si:In (Reference 8)

SECTION II

ABSORPTION MEASUREMENTS

1. EXPERIMENTAL PROCEDURE

The absorption samples were cooled to 5.5K in a liquid helium dewar during measurement. All spectra were recorded on a Digilab model FTS-20CVX Fourier transform spectrophotometer at a resolution of 1 cm^{-1} with signal averaging over 1,000 to 2,000 scans. Use of a cesium iodide (CsI) beamsplitter and a TGS detector with CsI window permitted investigation in the region from 4,000 to 200 cm^{-1} . The spectra were recorded in the single beam mode with the sample transmittance referenced to an empty sample holder. A computer program written by Rome was used to convert transmittance to absorption coefficient in the usual manner (Reference 9).

The samples were 12 mm by 12 mm by 1 mm in dimension. They were mounted in a stress-free manner by attaching them to the dewar coldfinger with a very small dab of conducting vacuum grease on one corner.

2. RESULTS AND DISCUSSION

Infrared absorption spectra of two different samples, labeled 0797 and 0798, were obtained at 5.5K. Samples 0797 and 0798 were side-by-side sections cut from the same wafer (Appendix A). The spectra of both samples are shown in Figure 4 for the region from 200 to 1300 cm^{-1} . Local mode absorptions are observed for interstitial oxygen and substitutional carbon at 1136 and 608 cm^{-1} , respectively. The excitation spectra of indium, aluminum, aluminum-x, and boron are also observed in both samples. The main difference between the two samples is the concentration of the various impurity centers as indicated in Table 2. Sample 0797 contains more aluminum, indium and oxygen, but less boron and carbon than sample 0798. The aluminum x-level concentration is the same for both. These concentrations were determined by measuring a peak area or peak height and multiplying by an empirical calibration factor as given in Table 3. Most of the calibration factors used were taken

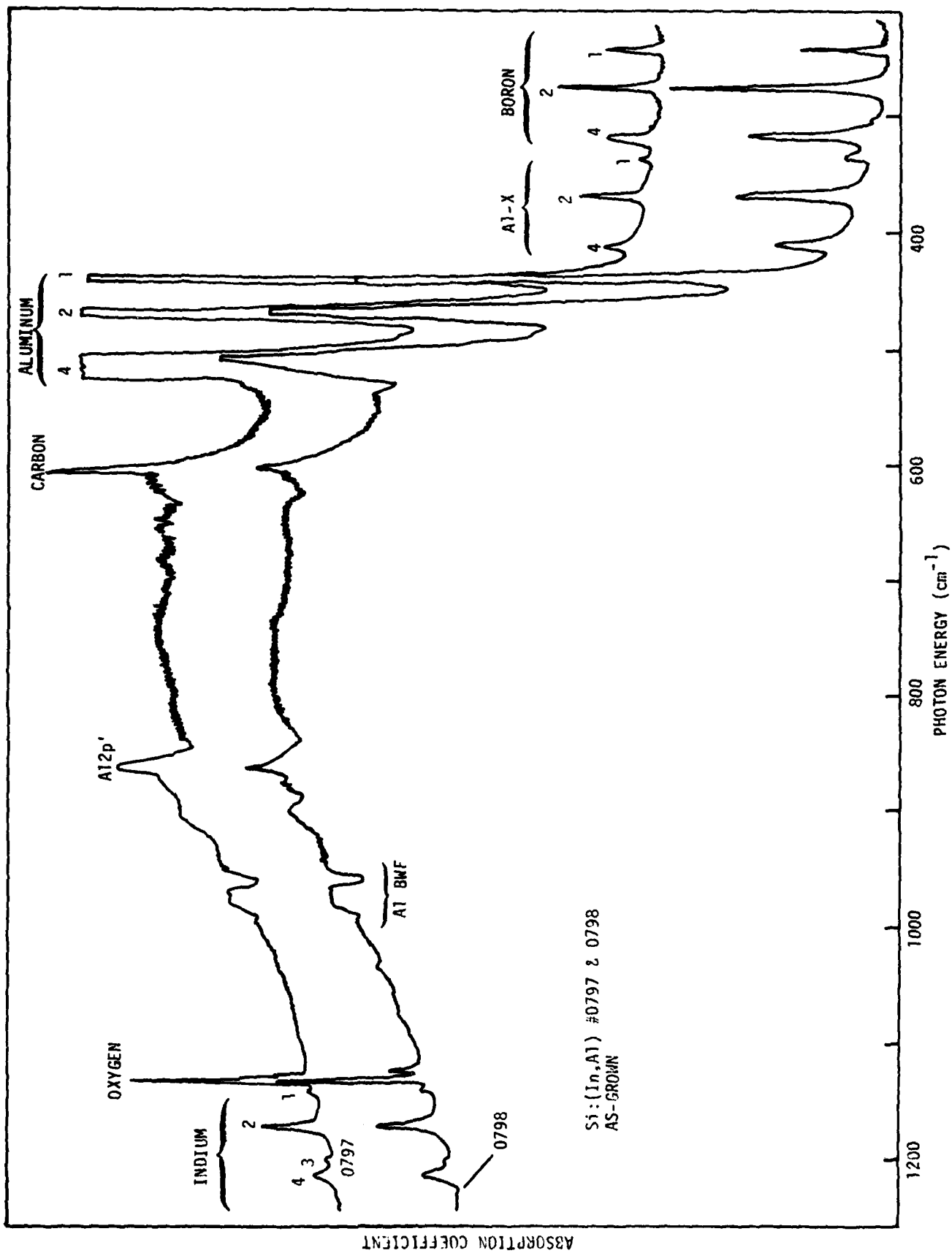


Figure 4. Infrared Absorption Spectra Of As-Grown Si:(In, Al) Samples 0797 And 0798

TABLE 2

IMPURITY CONCENTRATIONS DETERMINED BY IR ABSORPTION
FOR CZ Si:(In, Al) SAMPLES. CONCENTRATIONS ARE atoms/cm³.

SAMPLE	B	Al	Al-X	Al-X/Al	In	In-X	O	C
0797 as-grown	6.0×10^{14}	1.8×10^{16}	5.4×10^{14}	.030	6.0×10^{16}	$<10^{15}$	4.5×10^{17}	5.1×10^{17}
0797 annealed	3.5×10^{14}	1.8×10^{16}	2.7×10^{14}	.015	6.0×10^{16}	$<10^{15}$	8.1×10^{17}	3.3×10^{17}
0798 as-grown	6.8×10^{14}	7×10^{15}	5.3×10^{14}	.076	3.6×10^{16}	$<10^{15}$	1.8×10^{17}	8.0×10^{16}

Neutron Activation Analysis of Sample 0798 yielded $N_{In} = 3.4 \times 10^{16}$ atoms/cm³.

TABLE 3

CALIBRATION FACTORS USED TO DETERMINE CONCENTRATIONS
BY IR ABSORPTION^a. SAMPLE TEMPERATURE 5.5K

<u>LINE</u>	<u>CONCENTRATION</u>
Boron 2	peak area/ 6.6×10^{-14}
Aluminum 2p'	peak height $\times 2.8 \times 10^{15}$
Aluminum -X 2	peak area/ 4×10^{-14}
Indium 2	peak area/ 5×10^{-16}
Oxygen	peak height $\times 3.1 \times 10^{16}$
Carbon	peak height $\times 6.7 \times 10^{16}$

^aAll values except for Al2p' line are taken from Jones et al. (Reference 4)

from a paper by Jones et al. (Reference 4), but they are used with certain reservations to be discussed later. The concentrations listed in Table 2 seem to indicate that the distribution of the dopants and impurities is not homogeneous across the wafer.

Enlarged views of the indium, aluminum x-level and boron $P_{2/3}$ excitation spectra are shown in Figures 5 and 6. Wavelength positions and relative line intensities within each spectrum agree well with previous results (References 4, 10, 11). Notice, however, that only lines 1 through 4 are observed in each spectrum. There is no evidence of lines 5-11 for any of the four acceptor centers. Lines 1-4 are also broader than normal. In our experience, this sort of line broadening and the absence of lines 5-11 is usually due to one of three causes: a) external stress on the sample, b) a high ($>10^{17}$ atoms/cm³) acceptor concentration causing nearest-neighbor impurity wave functions to overlap,

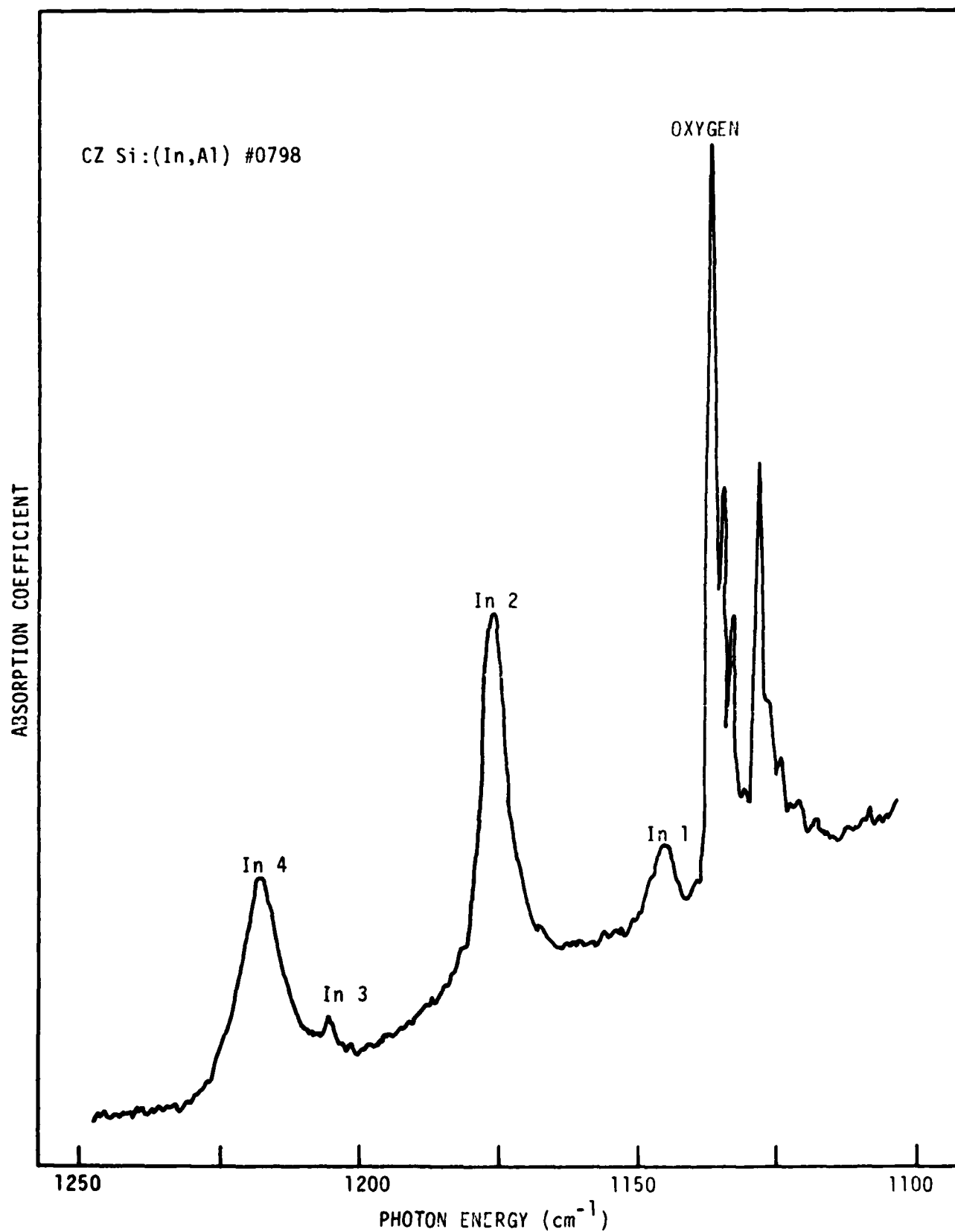


Figure 5. Infrared Absorption Spectrum Of Sample 0798 Showing The Indium $P_{3/2}$ Excitation Lines And The Oxygen Local Mode Absorption

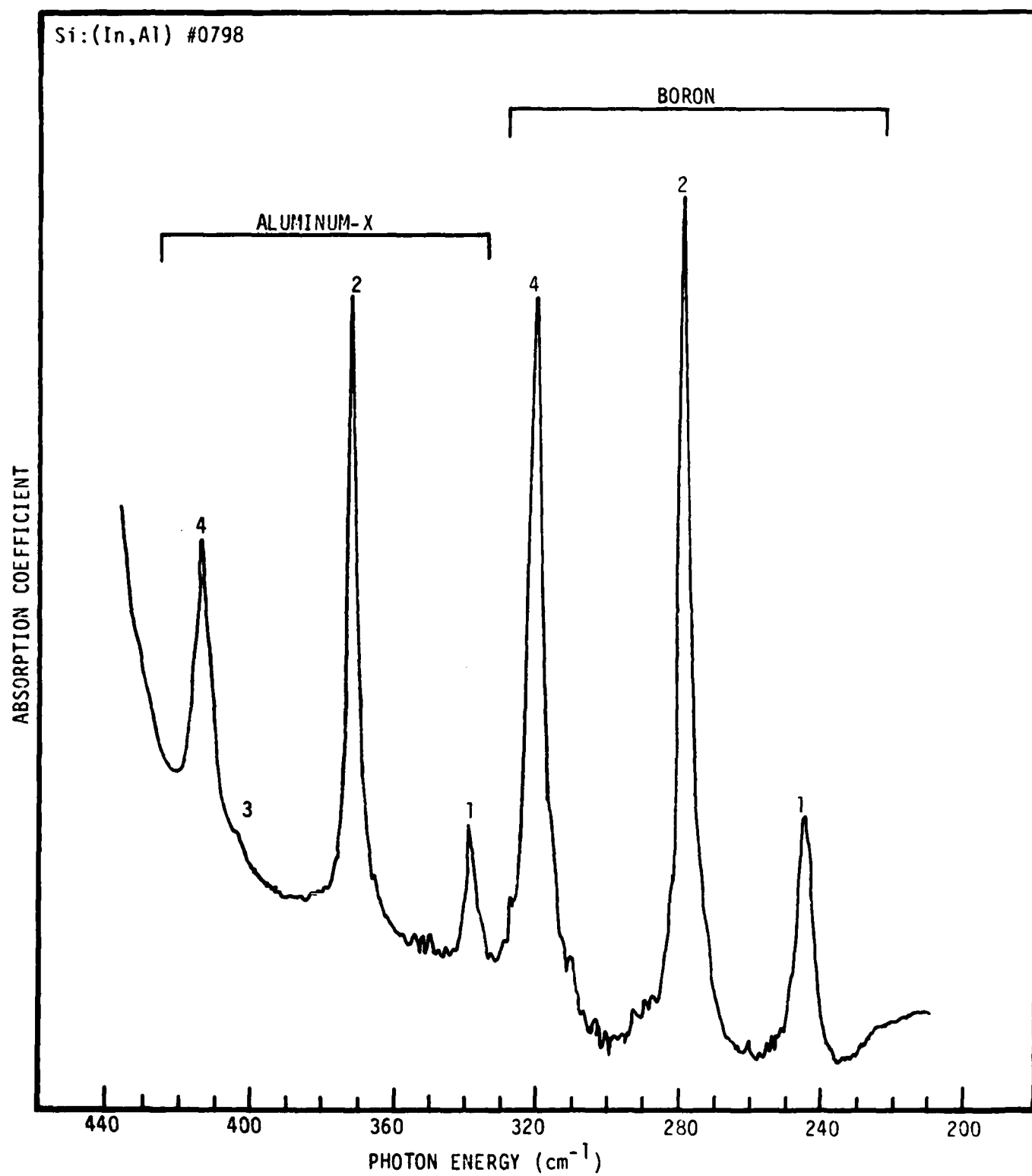


Figure 6. Infrared Absorption Spectrum Of Sample 0798 Showing Boron And Aluminum-X $P_{3/2}$ Excitation Lines

or c) lattice damage such as that caused by neutron irradiation. Reason (a) can be eliminated because several normally stress-free sample mounting procedures were tried with no change in the spectra. Reason (c) seems unlikely because annealing had no effect on line widths. This leaves reason (b), concentration broadening. According to Table 2, the total acceptor concentration is approximately 10^{17} atom/cm³ which may very well be sufficient to cause the observed broadening (Reference 12). Perhaps different acceptors are occupying nearest-neighbor sites and they may influence each other in a different manner than identical nearest-neighbor acceptors.

In Figure 6, the aluminum x-level spectrum is quite prominent. The observed lines are in good agreement with those published previously (References 4,13,14). As seen in Table 2, the aluminum x-level concentration is about 3 to 6 percent of the parent aluminum concentration in the as-grown samples which is considerably higher than that observed by previous workers (References 4,14). No indium x-level is observed in the absorption spectra. This is not too surprising considering the low cross-section and the fact that the indium x-level concentration is usually 0.1 percent or less of the indium concentration (References 4, 14). This could place it below the detectability limit (2×10^{15} for 1 mm sample) for the sample thickness used here. It should be noted, however, that we have some reservations about the absorption calibration factors used for the x-centers (Reference 4) because no x-center standards exist for calibration purposes. The only reasonable assumption that can be made is that the x-center cross-sections follow the same relationships as the normal Group IIIA acceptor cross-sections (Reference 4).

Some other comments concerning the Group III acceptor cross-sections are in order here. The concentrations listed in Table 2 were determined using the calibration factors listed in Table 3 which are taken from Jones et al. (Reference 4). Some recent work by Rome (Reference 15), however, has shown that these calibration factors are sometimes not very accurate when applied to our experimental set-up. Also, these calibration factors were determined for singly-doped silicon samples and some of our recent results (References 15,16) seem to indicate that they may not apply to multiply-doped samples. Perhaps different acceptors at high

concentrations influence each other in a way that could seriously affect the calibration factors. On the other hand, the indium concentration for sample 0798 as determined by absorption (3.6×10^{16} atoms/cm³ using the calibration factor of Jones et al. (Reference 4)) is in excellent agreement with the neutron activation analysis value of 3.46×10^{16} (sample 0798 was sent to the University of Missouri for neutron activation analysis after the absorption analysis was completed). Whether or not the other concentrations listed in Table 2 are as accurate as that of indium is unknown at this time. The boron and aluminum concentrations could not be determined by neutron activation analysis.

Sample 0797 was subsequently annealed twice. Each anneal consisted of 1/2 hour at 650°C followed by 4 hours at 600°C in an argon atmosphere. The annealing had an effect on the absorption spectra as shown in Figure 7 and Table 2. Neither the indium nor the aluminum concentrations changed after annealing but the concentrations of the other impurities did change. Both boron and the aluminum x-level decreased significantly after annealing. Carbon also decreased but oxygen increased by quite a bit. Neither spectrum shows any evidence of the formation of SiC or C-O complexes. The increase of oxygen may be related to a problem in maintaining the argon atmosphere during the first anneal such that ambient air may have come in contact with the heated sample. The reason for the decrease in the shallow boron and aluminum x-levels is not obvious at this point.

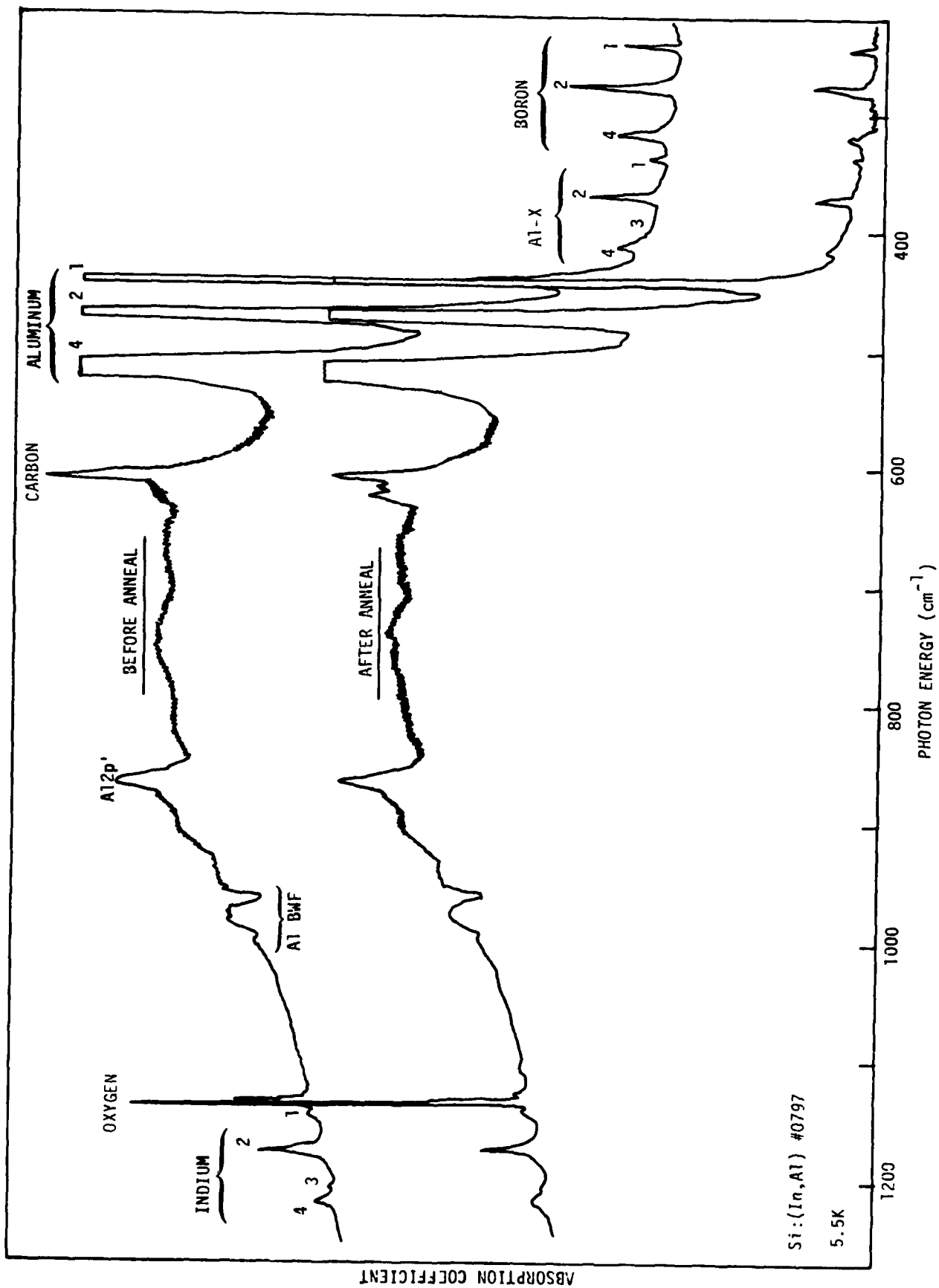


Figure 7. Infrared Absorption Spectra Of Sample 0797 Before And After Annealing

SECTION III

PHOTOCONDUCTIVITY MEASUREMENTS

1. EXPERIMENTAL PROCEDURE

Photoconductivity measurements were made on 3mm x 5mm x 1.4mm samples using the same Digilab FTS spectrometer as the absorption measurements. All spectra were recorded at a resolution of 2 cm^{-1} with 100-1,000 scans in the infrared region from 4,000 to 200 cm^{-1} . The photoconductivity measurements were made in voltage-mode with an applied DC electric field of 20 V/cm. The resulting voltage signal was fed through the existing detector electronics of the FTS spectrometer to be recorded and analyzed by computer. The samples were mounted on a thin beryllium oxide slab on the coldfinger of CTI Cryotronics model LTS-21 closed-cycle refrigeration system. Data was recorded at eight different sample temperatures in the range of 10.5K to 23.8K.

2. RESULTS AND DISCUSSION

Photoconductivity spectra of three different samples, labeled 0799, 0799' and 0800 (see Appendix A), were obtained at various sample temperatures. The spectra of samples 0799' and 0800 were very similar. However, the spectra of 0799, while also similar in many respects, showed no aluminum x-level excited state lines. In Figure 8 a typical photoconductive response curve for samples 0799' and 0800 at 20K is compared to an infrared absorption spectrum at 5.5K. The photoconductivity spectrum shows good agreement with the infrared absorption spectrum. Both spectra show lines 1-4 of the $P_{3/2}$ excited states of indium and aluminum at the same energy positions. Also line 4 of the $P_{3/2}$ excited states of boron and the aluminum x-level is shown in both spectra. In addition, the aluminum 2p' line and the local mode absorptions for substitutional carbon (608 cm^{-1}) and interstitial oxygen (1128 and 1136 cm^{-1}) are observed (see Appendix B). One difference between the two spectra is the additional aluminum BWF resonance lines (Reference 17) seen in the photoconductivity spectra. Photoconductivity is typically more sensitive to BWF resonance states than infrared absorption measure-

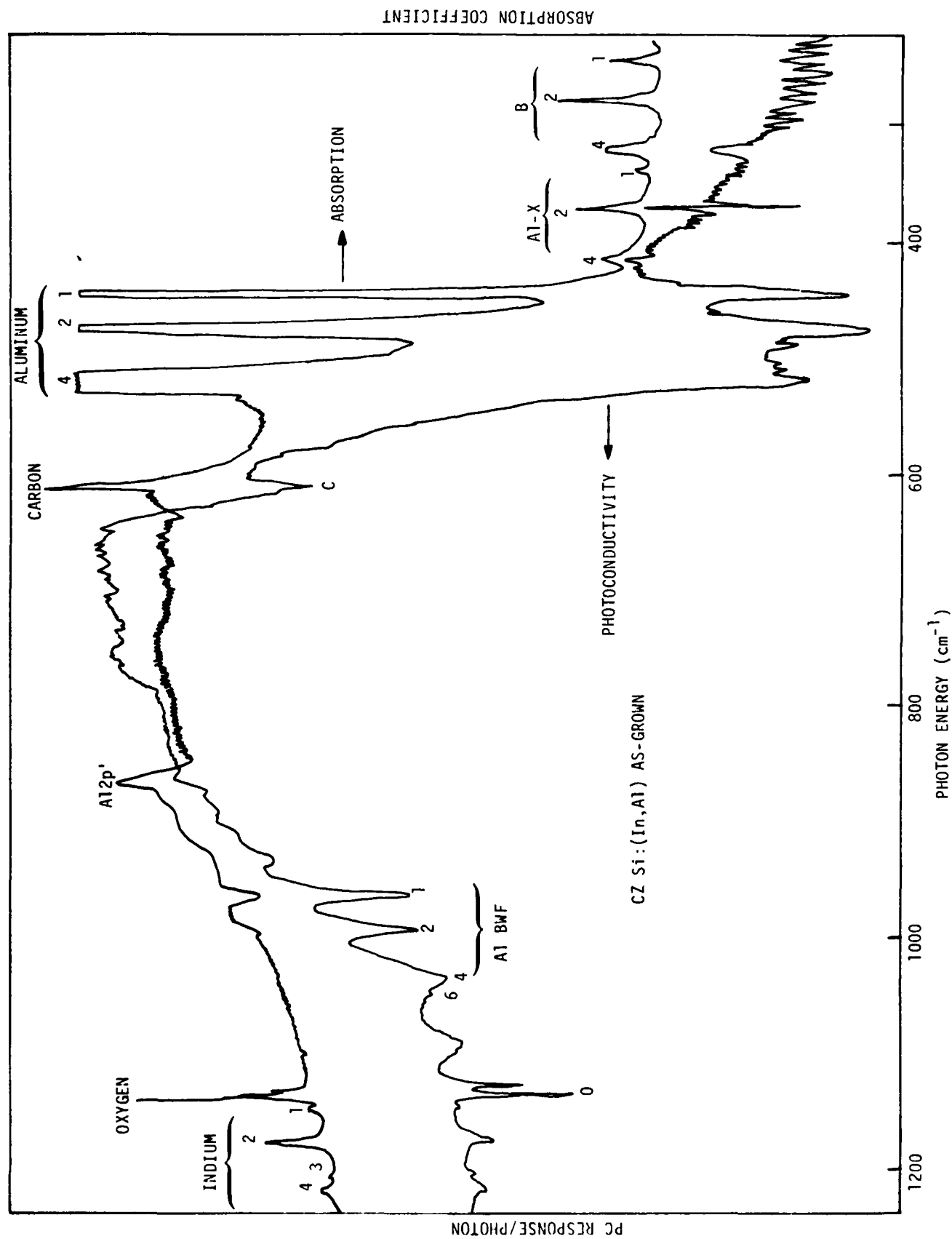


Figure 8. Photoconductivity And Infrared Absorption Spectra For As-Grown CZ Si:(In, Al)

ments. As mentioned previously, only lines 1-4 are observed in the spectra of these Si:(In, Al) samples. Unlike previous Si:In or Si:Al photoconductivity data (References 18,19), there is no evidence of excited state lines 5-10. Also, the line widths of lines 1-4 are broader than those seen in previous singly-doped samples. As discussed in Section II, these effects are most likely due to concentration broadening.

It is also interesting to note that in all the CZ Si:(In, Al) spectra obtained, the excited state lines 1-4 of indium and aluminum are seen as negative peaks even at sample temperatures up to 30K. This same phenomenon was observed for the indium excited state lines in FZ Si:(In, Al) and for the gallium excited state lines of Si:(Ga, B) (References 7, 19). Typically, in a singly-doped Si:In sample line 4 is a positive peak by temperatures around 12K (Reference 18). A positive excited state peak is the result of photothermal ionization (Reference 20) creating an extra hole in the valence band. A negative peak is the result of photoexcitation of a hole to an excited state without subsequent thermal ionization to the valence band. Hence, in a multiply-doped system the deeper acceptors appear not to thermally ionize to the valence band in the same temperature range as they do in a singly-doped sample. One possible explanation is that the rate of thermal ionization is lower than the photoionization rate of the shallower acceptor.

In contrast, the boron and aluminum x-level are photothermally ionized. Figure 9 shows how the excited state lines of these two acceptors change with increasing temperature. While the two boron lines are always seen as positive peaks, the aluminum x-level line 4 goes from a negative peak at 10.5K to a positive peak at 20K. The intensity of these three lines vs. temperature was analyzed following the technique used by Chandler et al. (Reference 18). By fitting the data to a simple exponential function the binding energies of the excited states can be determined as shown in Figure 10. Based on this exponential fit, the calculated binding energies are:

Boron line 2	$E_B = 10.0 \pm 0.3 \text{ meV}$
Boron line 4	$E_B = 4.8 \pm 0.3 \text{ meV}$
Aluminum-X line 4	$E_B = 5.1 \pm 0.4 \text{ meV}$

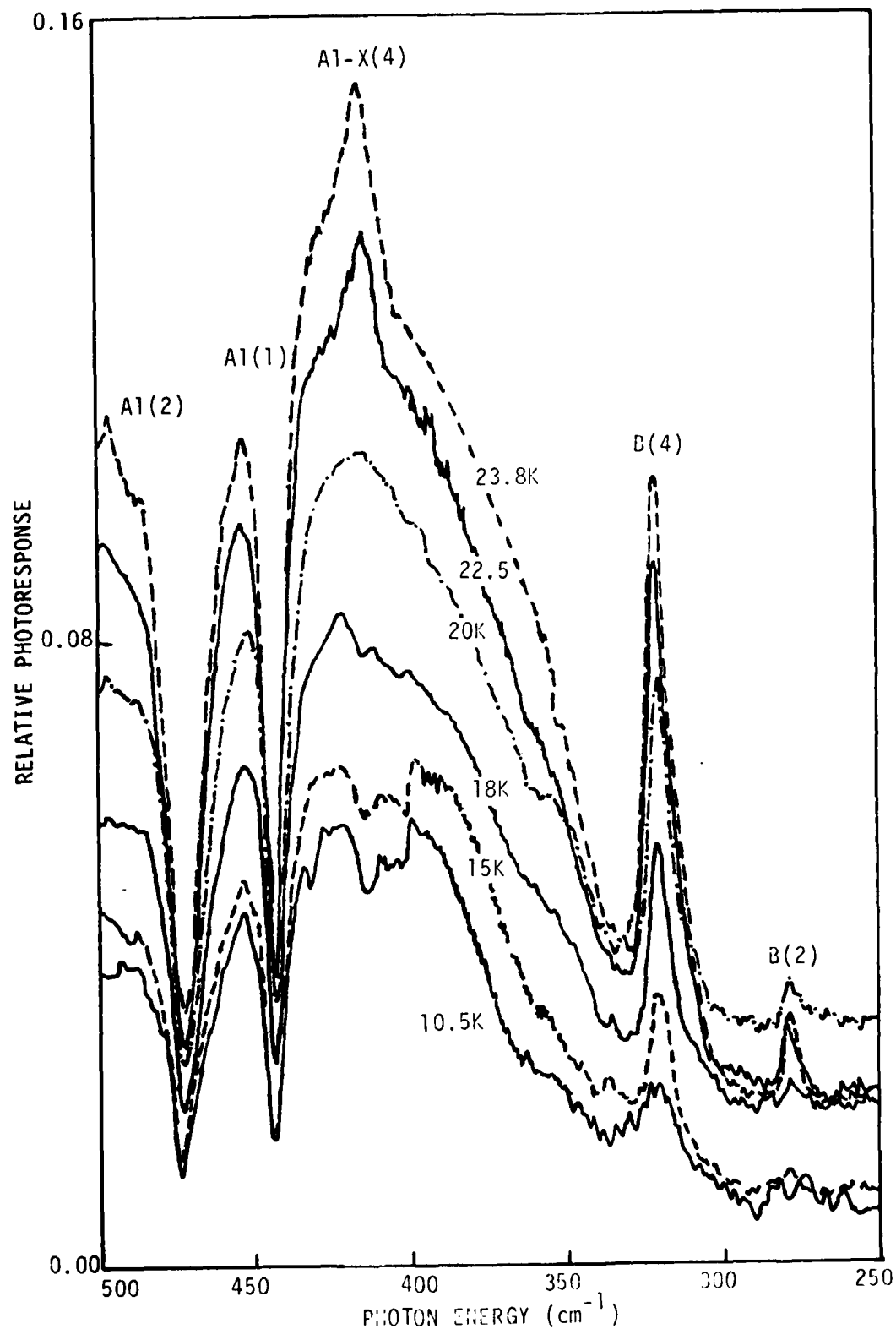


Figure 9. Temperature Dependence Of The Photothermal Ionization Of The Aluminum X-Level Line 4

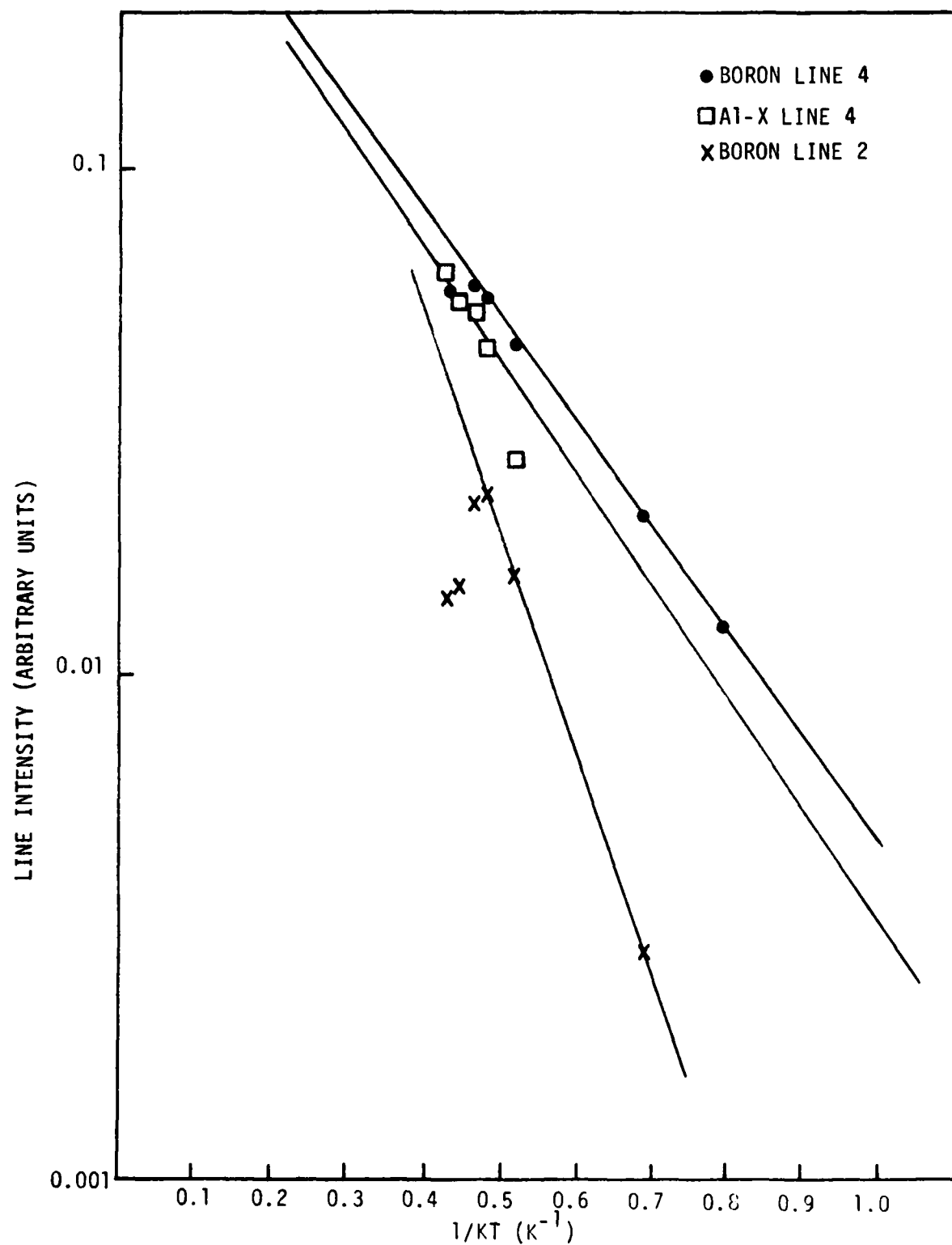


Figure 10. Aluminum X-Level Line 4 Intensity vs. Reciprocal Temperature

Based on absorption data by Fischer and Rome (Reference 11) and by Scott (Reference 13), the binding energies for these lines are:

Boron line 2	$E_B = 9.90 \pm 0.02 \text{ meV}$
Boron line 4	$E_B = 4.80 \pm 0.02 \text{ meV}$
Aluminum-X line 4	$E_B = 5.0 \pm 0.4 \text{ meV}$

This good agreement between the thermally determined binding energies and the optically determined binding energies is expected for the photothermal ionization process. Hence, the aluminum x-level behaves as a simple acceptor in silicon and undergoes the same photothermal ionization process. A similar result was seen previously for the gallium x-level (Reference 19).

The next step in the study of the aluminum x-level was to anneal sample 0799' at 650°C for 1/2 hour followed by 4 hours at 600°C. Figure 11 compares the photoconductivity results for 0799' before and after annealing. The major difference is the absence of any boron or aluminum x-level response in the after anneal spectrum. Absorption data showed a factor of two decrease in the boron and aluminum x-level concentrations after annealing. However, the boron and aluminum x-level lines were still clearly seen by absorption after the anneals. It is unclear why the photoconductive response shows no evidence for the boron or aluminum x-level impurities observed in the absorption spectrum after anneal. The Hall data showed an increase in the number of donors after annealing so it is possible that these two shallow levels have become compensated. However that would still leave a question as to why the levels are observed in the absorption data.

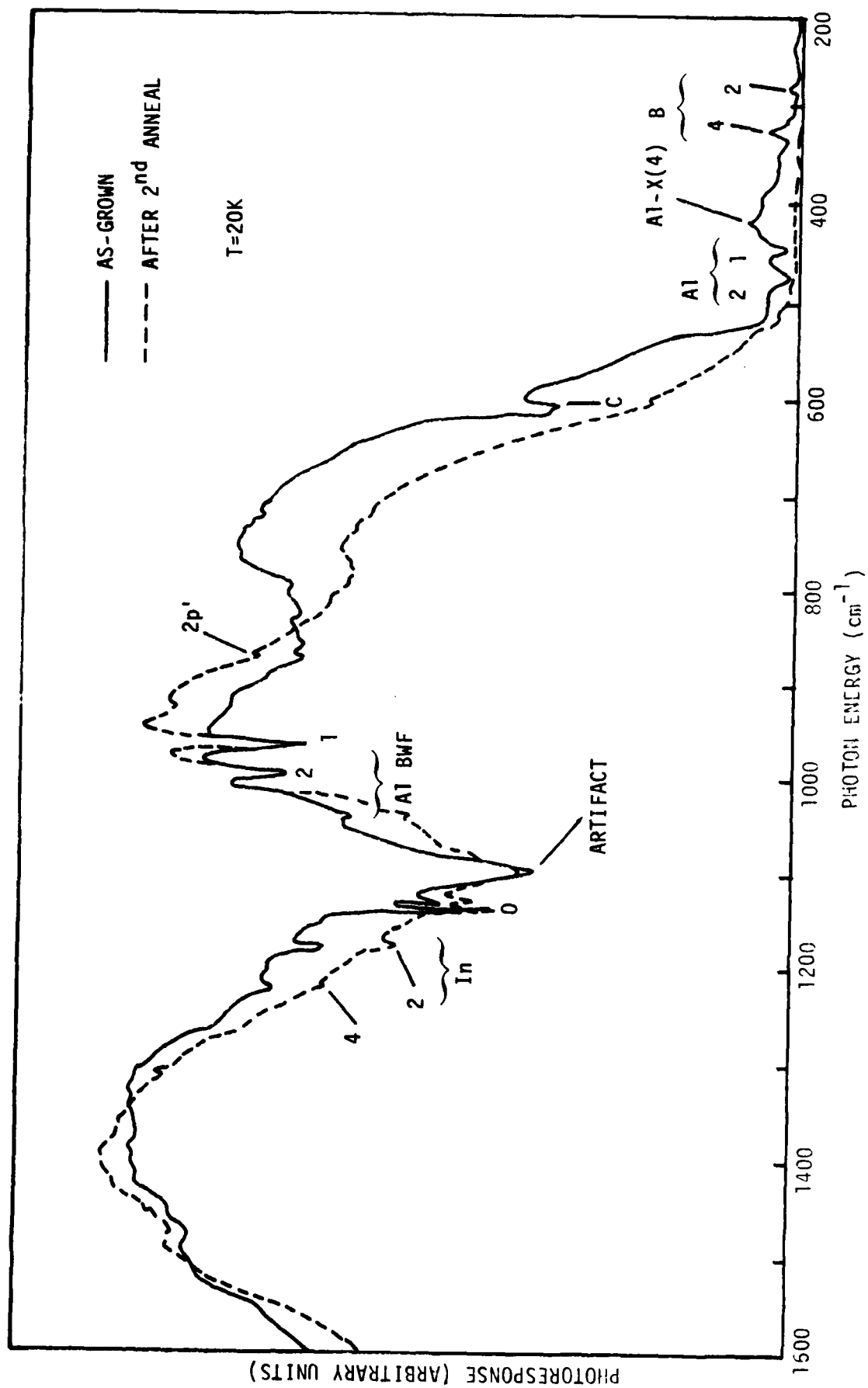


Figure 11. Photoconductivity Spectra Of Sample 0799' Before And After Annealing

SECTION IV

PHOTOLUMINESCENCE MEASUREMENTS

1. EXPERIMENTAL PROCEDURE

The experimental procedure for the photoluminescence measurements has been described previously (Reference 7).

2. RESULTS AND DISCUSSION

Photoluminescence spectra of the same two samples used for absorption, 0797 and 0798 (See Appendix A) were recorded. Figure 12 shows luminescence from sample 0797 after the two annealing stages. This spectrum is practically identical to that obtained before annealing. The main bound exciton features, due entirely to indium, are labeled on that spectrum. Aluminum bound exciton features are not observed, nor are there any lines characteristic of isoelectronic centers. The lack of aluminum-related luminescence is to be expected based on previous work on float-zoned Si:(In, Al) (Reference 7) and other dual-acceptor systems where the exciton tunneling mechanism is active.

Assuming that the pair models postulated for x-level acceptors and the U_2 defect in silicon (acceptor-carbon (References 3,21) and Fe-In pairs (Reference 22), respectively) are correct, then it seems clear that Al-C pairs are formed in this material at the expense of In-C and In-Fe pairs. This result stands in contrast to evidence obtained from related studies of float-zoned Si:(In, Al) (Reference 7) where In-Fe pairs formed preferentially to In-C and Al-C pairs.

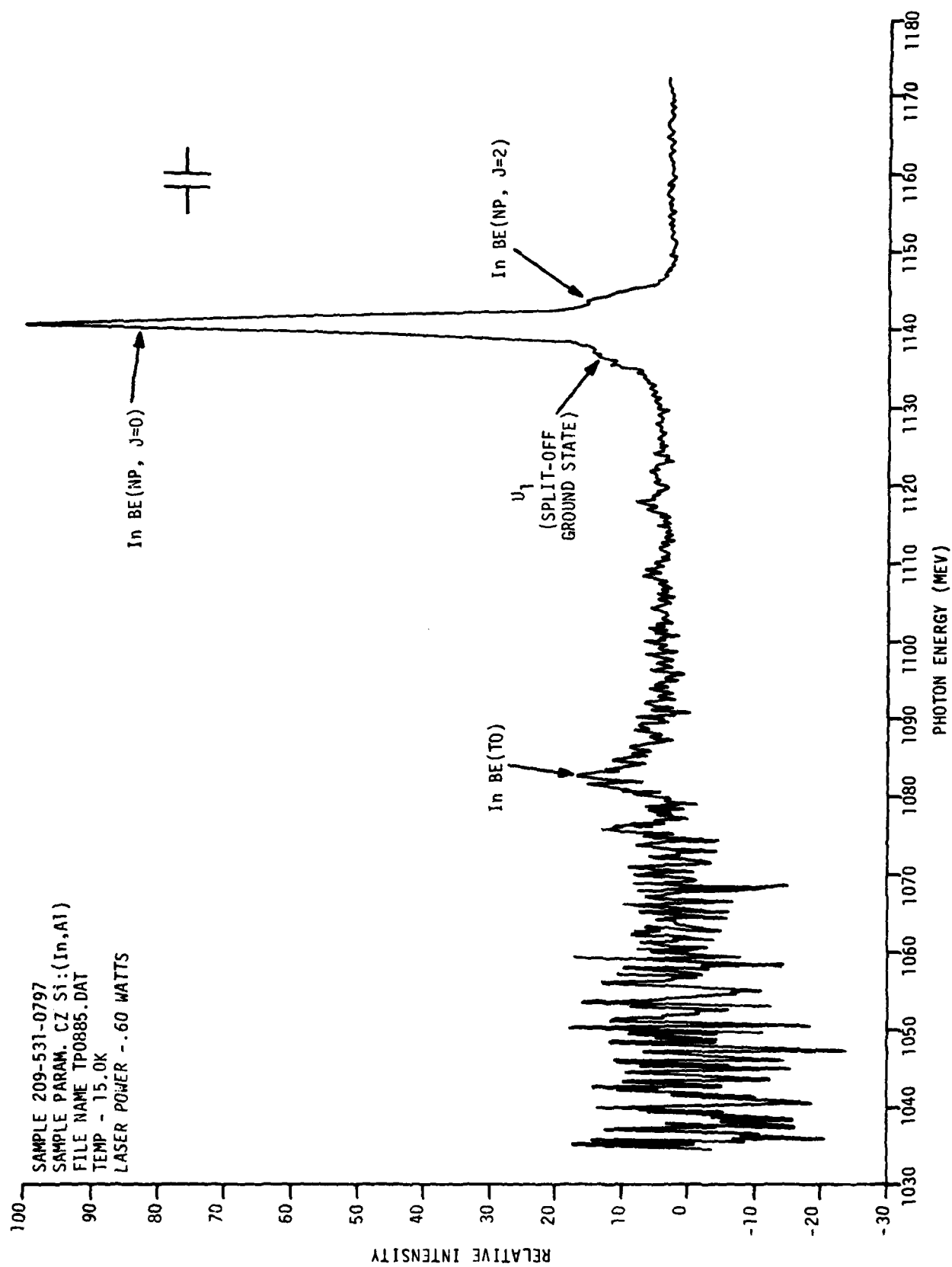


Figure 12. Photoluminescence Of As-Grown CZ Si:(In, Al) Showing Indium Bound-Exciton Features

SECTION V

HALL EFFECT MEASUREMENTS

1. EXPERIMENTAL PROCEDURE

Hall effect transport data were taken on a guarded DC Hall apparatus designed for high impedance ($\sim 10^{13} \Omega$) measurements (Reference 23). The samples were cut into a cloverleaf shaped van der Pauw configuration and ohmic contact areas were produced by pulsed laser annealing of regions coated with borosilicate (Reference 24).

The samples were held in a cryogenic variable temperature dewar and subjected to an applied magnetic field of one-half Tesla. Data analysis procedures have been described previously (Reference 25). In the charge-balance equation used to fit the net carrier concentration versus $1/T$ curve, the density of states in the valence band, N_V , was calculated taking into account the temperature dependence of the carrier concentration effective hole mass which results from the non-parabolicity of the valence bands (References 25,26). A degeneracy factor of $g=4$ was used for all dopants. An empirical Hall scattering factor ($r \neq 1$) (Reference 27) was also used which results in closer agreement with carrier concentrations obtained from C-V measurements and with optically determined acceptor ionization energies (Reference 28).

2. RESULTS AND DISCUSSION

Three samples, 0795-I, 0795-II and 0796, were cut from the same wafer of Czochralski grown Si:(In, Al) material (see Appendix A). Transport data were collected and the measured carrier concentration as a function of temperature was fitted by a standard procedure using an interactive computer program. Initial concentration estimates of the known dopants and the compensation are entered as parameters into the charge balance equation and used to calculate carrier concentration. The impurity and dopant concentrations and the respective activation energies are then varied in an iterative search for minimization of the difference between the measured and calculated carrier concentrations at each measured

temperature by finding the minimum in χ^2 . A $\chi^2=1$ represents an acceptable fit which is based upon a 3% scatter in the data. If χ^2 is significantly higher, i.e. ten or greater, the fit is considered poor and additional impurities are included in the starting estimates. The dopant concentrations and activation energies resulting from the fit must be "reasonable," that is to say the energies must be close to known values and the concentrations must not exceed concentrations that would result in degeneracy. Occasionally the program will give a false minimum when the starting estimates are very wrong and/or when the data for whatever reason are especially noisy. In some cases it is helpful to hold the activation energies fixed, particularly when a dopant is overcompensated. The results of the Cz grown Si:(In, Al) impurity concentration fits for three samples from the same wafer are given in Table 4.

The as-received material exhibited non-uniformity from sample to sample, as indicated by the three different impurity concentration results. Sample 0795-I appears the most different but it also gave the most reasonable fitted values without fixing the activation energies (fixed activation energies are indicated in Table 4 by F). Sample 0795-I was selected for the annealing study described below.

The sample labeled 0795-I was subsequently annealed and run on the Hall system. The results after this first anneal were virtually identical to the as-grown material. Since there had been a problem with the ambient of the furnace possibly being contaminated by outside air, we decided to re-do the anneal and to run the sample again. The Hall results after the second anneal are presented in Table 5. The two columns labeled annealed represent two separate fits of the same data. The first fit gave the lowest χ^2 , but the number of donors (N_D) appears to have doubled after an annealing that should have reduced the donors. This result is entirely unexpected and increases the doubt in the fit. Consequently a second fit was made of the data by fixing the impurity activation energies. However this fit shows the boron concentration decreasing after annealing when the concentration should have remained relatively constant. One possible explanation for the difficulty in fitting the Hall data is that the high number of donors and acceptors present could make the r-factor less accurate and introduce errors into the fits. Additionally, the

TABLE 4
HALL EFFECT CONCENTRATION VALUES FOR AS-GROWN CZ Si: (In, Al)
(F implies fixed energies)

Impurity & Activation Energy	0.795_{-3}^{+1} (cm^{-3})	0.795_{-3}^{+11} (cm^{-3})	0.796_{-3} (cm^{-3})
Donors	2.3×10^{15}	8.84×10^{14}	1.07×10^{15}
Indium EA	5.75×10^{16} 0.165 eV	2.37×10^{16} 0.156 eV F	2.22×10^{16} 0.156 eV F
Aluminum EA	7.23×10^{16} 0.0644 eV	2.87×10^{16} 0.068 eV	3.59×10^{16} 0.0685 eV F
Boron EA	5.87×10^{15} 0.044 eV	1.20×10^{15} 0.0413 eV	2.18×10^{15} 0.0444 eV F
Al-X EA			
x^2	0.45	0.62	1.86

TABLE 5
HALL EFFECT CONCENTRATION VALUES FOR SAMPLE 0795-I, AS-GROWN AND POST-ANNEAL

Impurity & Activation Energy	As Grown (cm^{-3})	Annealed (cm^{-3})
Donors	2.30×10^{15}	4.54×10^{15} 3.80×10^{15}
Indium E_A	5.75×10^{16} 0.165 eV	3.76×10^{16} 0.147 eV 5.96×10^{15} 0.156 eV F
Aluminum E_A	7.23×10^{16} 0.0644 eV	4.44×10^{16} 0.0673 eV 8.08×10^{16} 0.0685 eV F
Boron E_A	5.87×10^{15} 0.044 eV	3.63×10^{15} 0.04439 eV F
Al-x E_A		2.6×10^{16} 0.0575 eV
x2	0.45	0.21 2.54

concentration of Al, which is the shallower dopant, exceeds the In concentration which makes it harder to accurately measure N_{In} .

Because of the difficulty in fitting the CZ Si:(In, Al) data, several composite graphs were made comparing the three CZ Si:(In, Al) samples and a previously run (Reference 7) FZ Si:(In, Al) sample. The FZ Si:(In, Al) sample did not exhibit any fitting problems and had much lower concentrations of aluminum, boron, and donors, and the In concentration exceeded that of Al. The first composite graph (Figure 13) is the hole concentration vs. $1000/T$ (K). In the FZ sample the exhaustion of the aluminum is very pronounced as demonstrated by the shoulder occurring at about $8(T^{-1})$, which illustrates that the Al concentration is less than that of the indium. The rise at the high temperature end is due to the indium activation. The CZ samples on the other hand have a higher concentration of all the dopants, particularly aluminum such that the shoulder structure is not apparent. This makes the exact determination of an indium concentration difficult. Even among the CZ samples, there is quite a bit of variation. This could indicate variations within the bulk of the material such as swirls or concentration gradients. These concentration variations are even more apparent on the other composite graphs, particularly the Hall mobility vs. T and $1000/T$.

In the Hall mobility graphs (Figures 14,15) the FZ material has a much higher mobility at lower T than does the CZ material. But the most interesting feature of these two graphs is the non-uniformity of the CZ material. The various degrees of tailing of the low temperature data indicate differences in the material from sample to sample on the same wafer.

However, with the Hall coefficient and the resistivity vs. $1000/T$ graphs (Figures 16,17), there is nothing singularly spectacular about the comparison of the four samples. The central region is almost the same for all the samples with divergence at both ends of the temperature runs.

Since there was difficulty in fitting the Cz Si:(In, Al) data, the possibility existed that the thicker than normal sample (1 mm vs. 20 mils) had a non-uniform current distribution. This would cause an

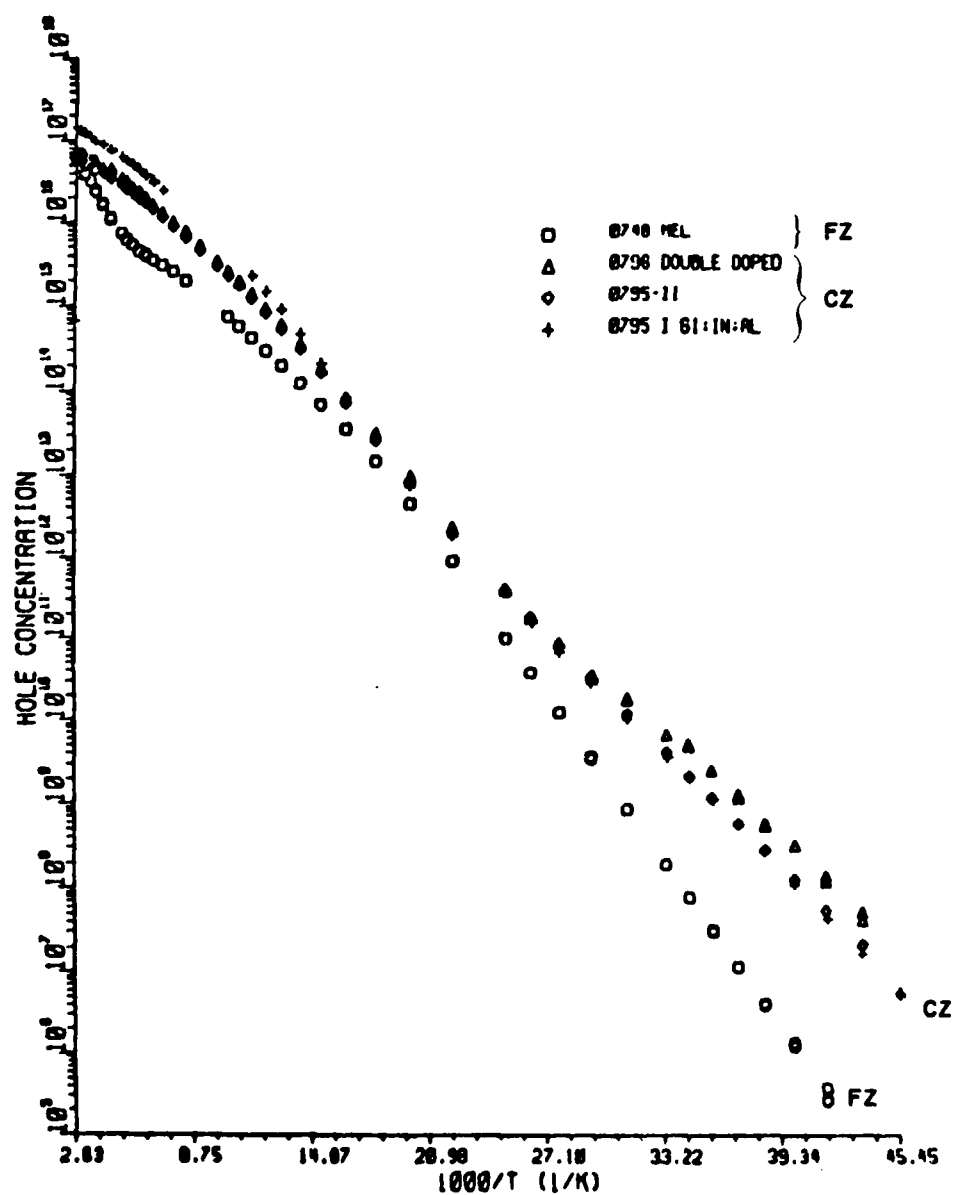


Figure 13. Hole Concentration vs. $1000/T$ For (Δ) As-Grown CZ Si:(In, Al), (\diamond) Annealed CZ, And FZ Si:(In, Al) Samples

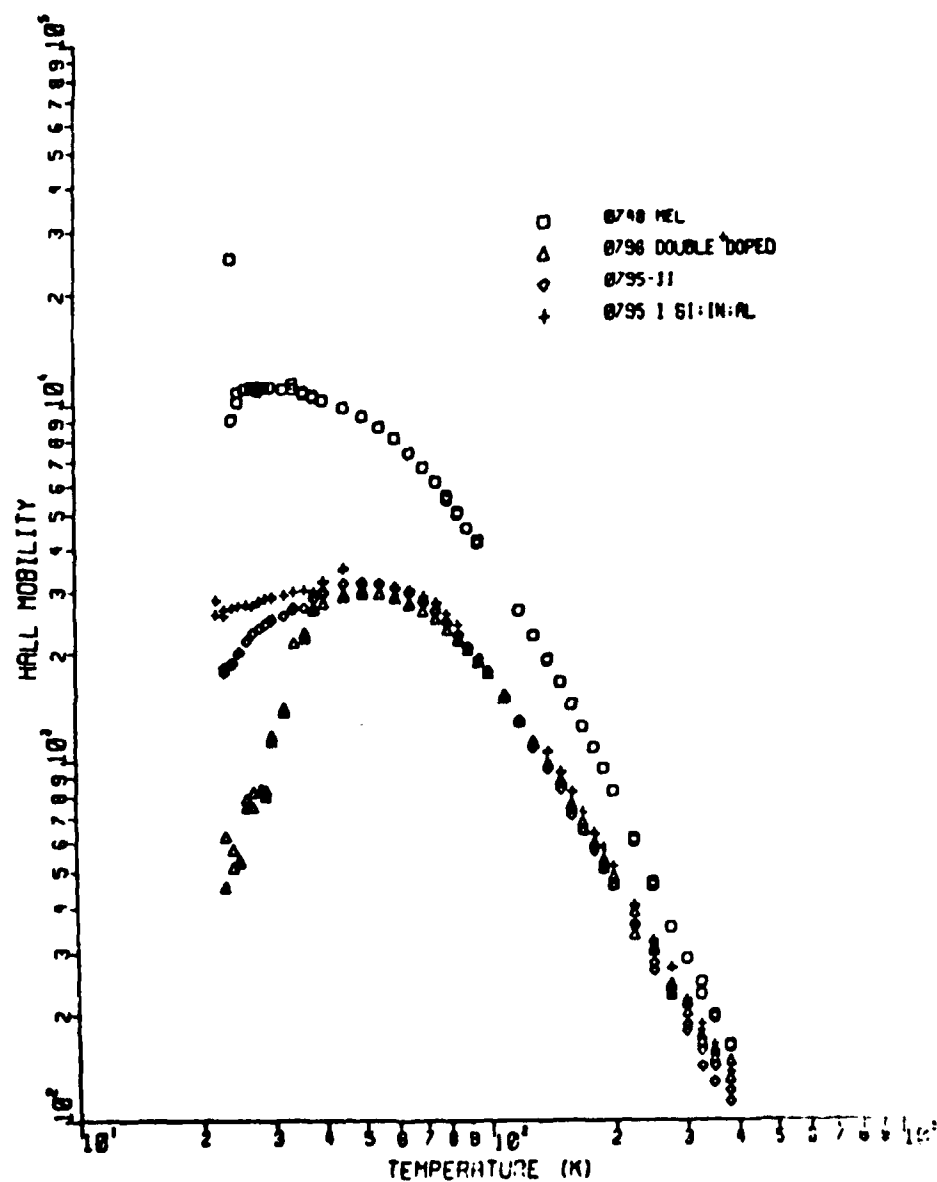


Figure 14. Hall Mobility vs. Temperature For (△) As-Grown CZ Si:(In, Al), (◇) Annealed CZ, And FZ Si:(In, Al) Samples

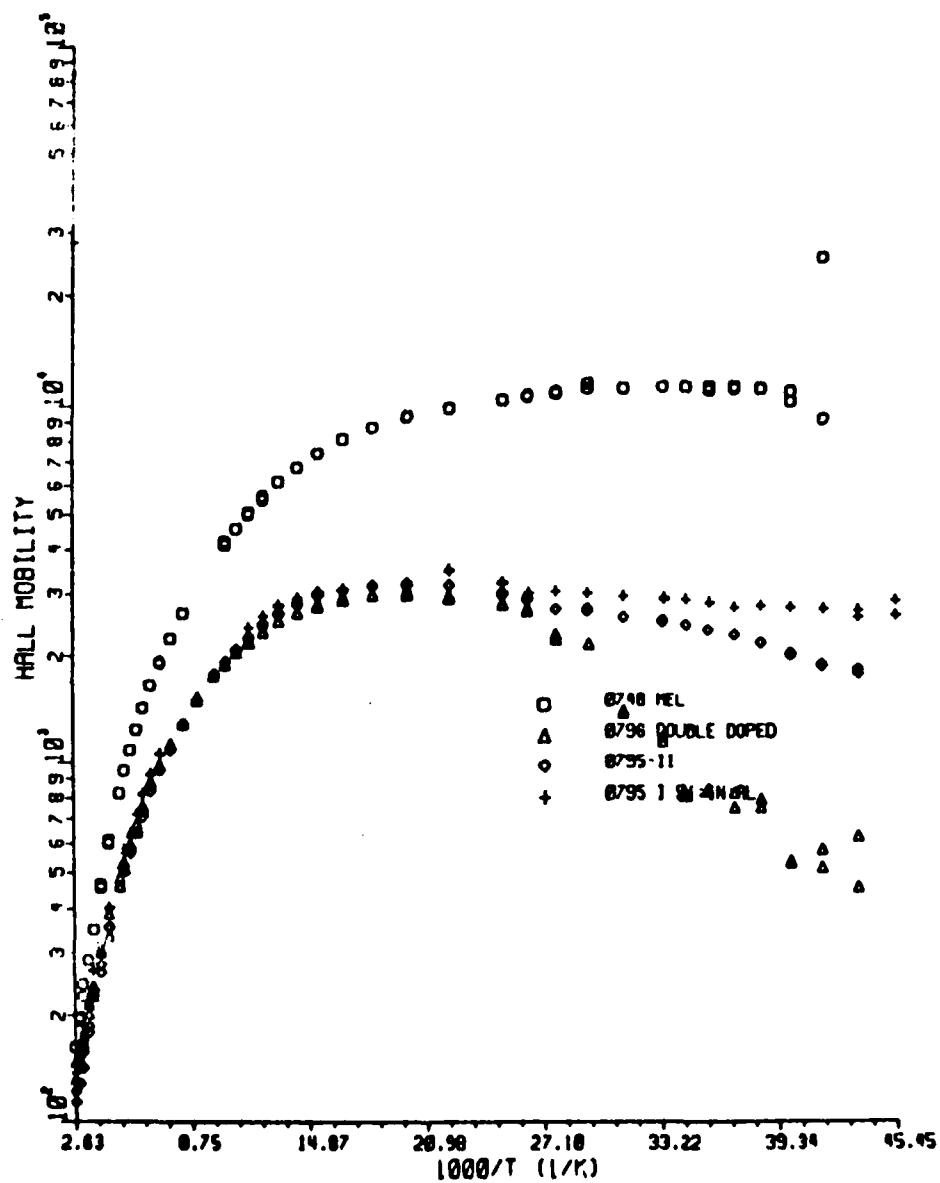


Figure 15. Hall Mobility vs. $1000/T$ For (Δ) As-Grown CZ Si:(In, Al), (\circ) Annealed CZ, And FZ Si:(In, Al) Samples

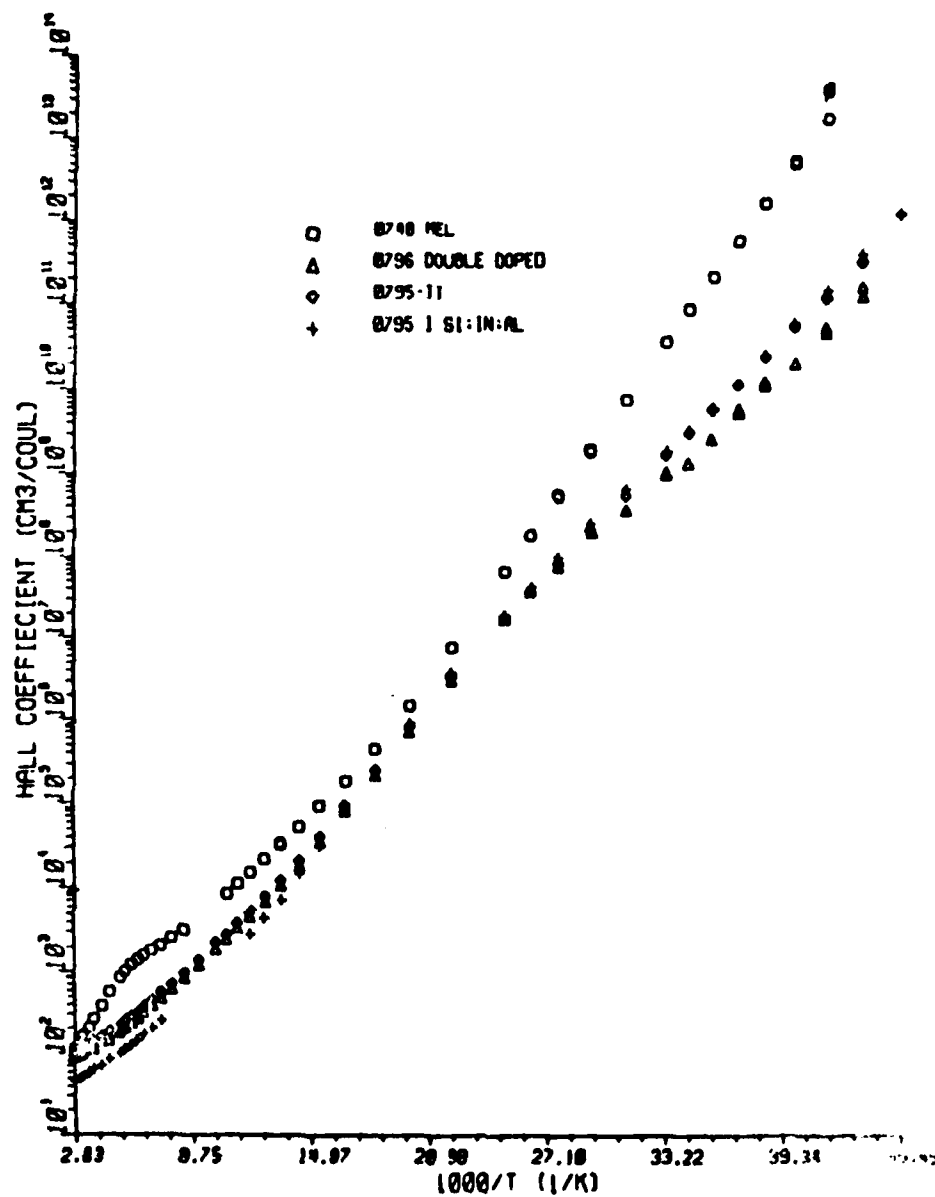


Figure 16. Hall Coefficient vs. $1000/T$ For (Δ) As-Grown CZ Si:(In, Al), (\diamond) Annealed CZ, And FZ Si:(In,Al) Samples

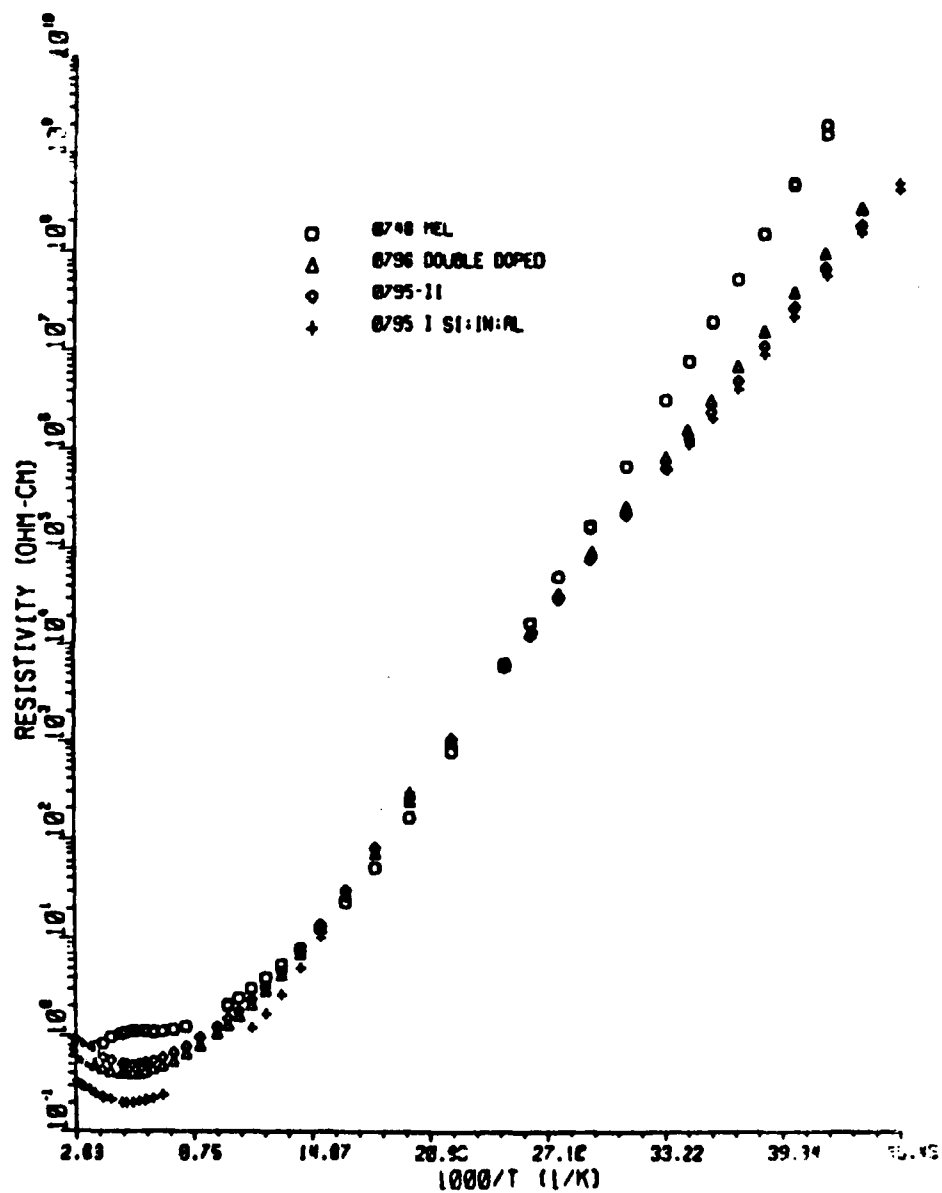


Figure 17. Resistivity vs. 1000/T For (△) As-Grown CZ Si:(In, Al), (◇) Annealed CZ, And FZ Si:(In, Al) Samples

incorrect determination of the donors and acceptors, due to the effective thickness being different from the actual, physical, thickness. The sample was thinned to 20 mils by polishing the back surface of the VDP sample. The sample was then cleaned in RCA solution II to remove any heavy metal contaminants and then in solutions I and II to remove any greases or oil. The sample was then run on the Hall system, described earlier and the results fitted.

The results for the thin sample were little different from the thick sample (see Table 6). What is of note is the comparison plots of all the runs plotted on common axes (see Figure 18). The curves have the appearance of what is expected when varying surface charges are applied to a sample, as in a surface treatment study of thin films on an insulator (Reference 29). This behavior of the sample with thickness suggested the possibility of defects acting as charge centers. To determine if this was the case a preferential etchant for silicon was used (Wright etch, Reference 30).

TABLE 6

HALL EFFECT CONCENTRATION VALUES FOR SAMPLE 0795-I, BEFORE
AND AFTER POLISHING TO THIN THE SAMPLE

IMPURITY & ACTIVATION ENERGY	1mm THICK (cm^{-3})	20 mils THICK (cm^{-3})
Donors	4.54×10^{15}	6.97×10^{15}
Indium E_A	3.76×10^{16} 0.156 eV F	3.29×10^{16} 0.156 eV F
Aluminum E_A	4.44×10^{16} 0.0673 eV	7.42×10^{16} 0.0671 eV
Al-X E_A	2.6×10^{16} 0.0575 eV	1.11×10^{16} 0.0546
x^2	0.21	1.46

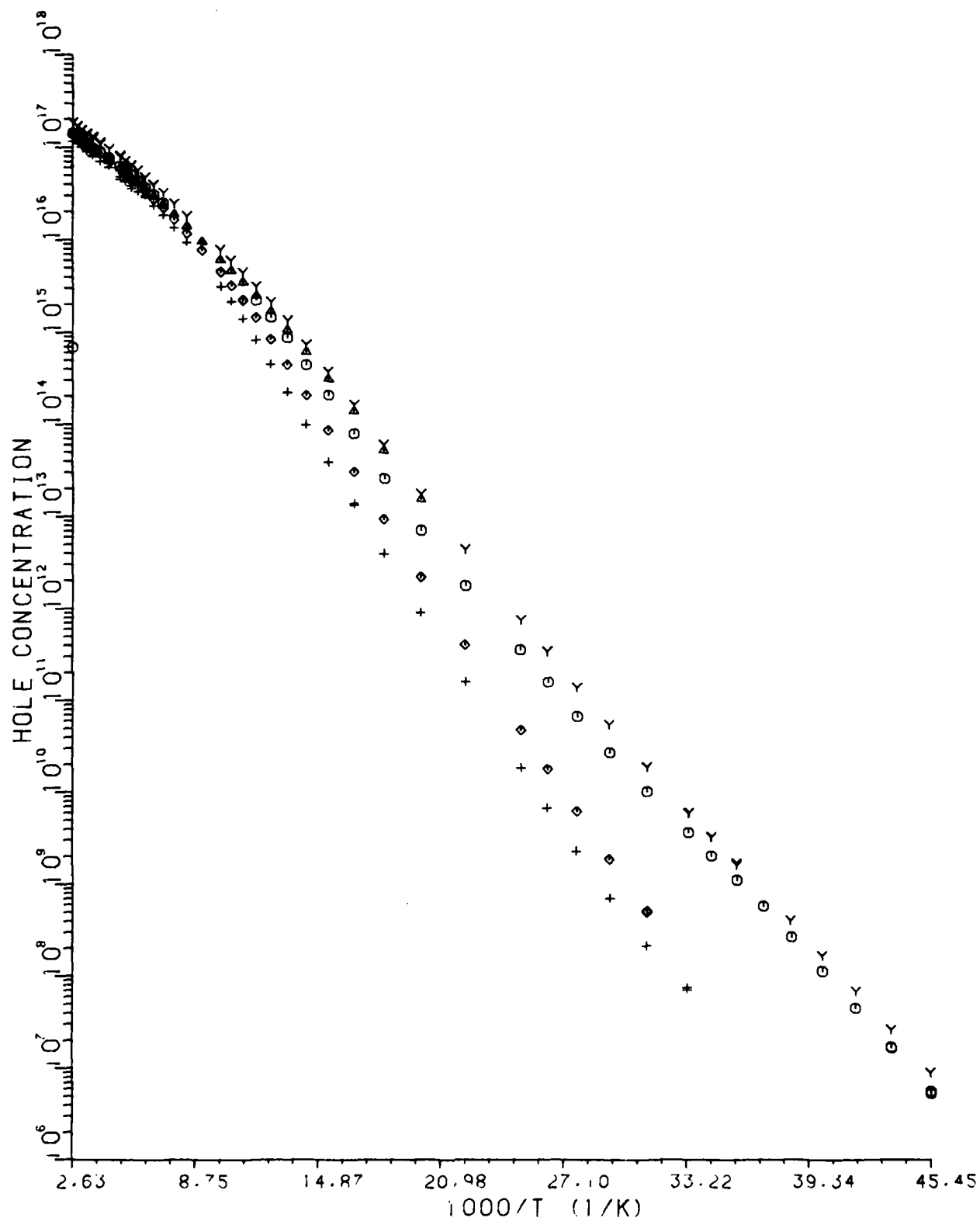


Figure 18. Hole Concentration vs. $1000/T$ For Sample 0795-I:
 (Y) As Grown, (O) After First Anneal, (Δ) Second
 Run After First Anneal, (\diamond) After Second Anneal, And
 (+) Thinned Sample

Sample preparation consisted of 30 second bath in 50:1 DI $H_2O:HF$, to strip the silicon of surface oxides. The sample was then placed in a 7:3 solution of heated $H_2SO_4:H_2O_2$ for 10 minutes to provide a chemically clean surface. The sample was then placed in Wright etch for the recommended time.

The surface had many cylindrical etch pits of an unusual shape as well as scratches. The pits were not of a standard variety and it was felt that the defects were actually defects caused by surface polishing. The sample was placed in CP4 for one minute to etch the surface damage.

Triangular etch pits were left after the CP4 etch. This was an indication of (111) etching. The density of defects was on the order of $1 \times 10^4/cm^2$. This is above what is considered good quality crystalline material, but it is not high enough to cause an adverse effect on the carriers. There was a large swirl or impingement defect between the contact region and the sample region. Its defect level was on the order of $1 \times 10^7/cm^2$, quite a large number. This would not in and of itself account for the difference in the results, but there was also what appeared to be a fine crack running across the sample area on the back surface. The CP4 had stained it so it was easily traced to a cutout region of the sample area (see Figure 19). It does not go through the entire sample but it could indicate a region that would have a resistivity temperature dependence different than other parts of the crystal which could cause difficulty in ascertaining the correct carrier concentration.

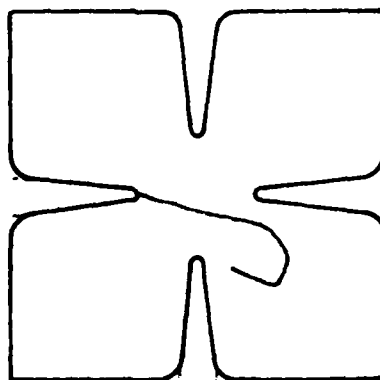
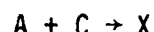


Figure 19. Location Of Crack On Thinned van der Pauw Sample 0795-I

SECTION VI

CONCLUSIONS AND RECOMMENDATIONS

The most striking feature of the results from our CZ Si:(In, Al) samples is the formation of a large concentration of Al-X at the expense of In-X and In-Fe pairs. Assuming the reaction mechanism for x-acceptors in Si to be



one may write the equilibrium constant at temperature T as

$$K(T) = \frac{[X]}{[A][C]} = K_0 \exp (\Delta H/KT)$$

where K_0 is related to the entropy of formation of X, ΔH is the enthalpy of formation, T is the absolute temperature, and k is the Boltzmann's constant. Using concentrations determined from the absorption measurements and values of K_0 and ΔH from Arch and Schafer (Reference 31), one may calculate the concentration of In-X and Al-X expected in CZ Si:(In, Al) after a 600°C anneal. Those expected values are:

$$[\text{In-X}] = 5.5 \times 10^{13} \text{ cm}^{-3}$$

$$[\text{Al-X}] = 5.7 \times 10^{13} \text{ cm}^{-3}$$

Obviously, the concentration of Al-X actually obtained is about a factor of 10 higher than would have been expected. No In-X was observed by Hall effect or absorption (although the expected concentration is below the detectability limit) in this study, and no Fe-In nor Al- related isoelectronic defect luminescence was observed.

Using published diffusion coefficients (Reference 32), one may calculate effective diffusion coefficients at 600°C for the impurities and dopants relevant for the formation of X-levels and acceptor-ion pairs; those results are summarized in Table 7.

TABLE 7
DIFFUSION COEFFICIENTS IN SILICON

	Al (cm ² /sec)	In (cm ² /sec)	C (cm ² /sec)	O (cm ² /sec)	Fe (cm ² /sec)
T = 600°C	7.4×10^{-20}	4.7×10^{-22}	3.1×10^{-18}	3.8×10^{-16}	5.71×10^{-8}
T = 1400°C	2.8×10^{-10}	2.9×10^{-11}	4.3×10^{-10}	4.5×10^{-9}	1.4×10^{-5}

Obviously, mobility of C, O, and Fe to the two dopants is not a problem in forming X and isoelectronic defects at 600°C and it is clear that Fe should pair the most rapidly as its diffusion coefficient is 8 orders of magnitude higher than the next most rapid diffuser. The critical effect describing the formation of Al-X over isoelectronic defects (such as In-Fe) is probably the binding energy of the relevant defects. The U₂ defect anneals at a very low temperature (Reference 33) and the rate of cooling after annealing was not sufficiently rapid to lock the Fe into the next-nearest neighbor interstitial site required for the U₂ defect. It has been shown that equilibrium concentrations of X-centers take much longer to form in FZ than in CZ silicon (Reference 4). Although oxygen is not believed to be a constituent in X-centers in Cz Si, it may facilitate the formation of those centers in Cz Si. The question of why Al-X forms instead of In-X is still unanswered. However, the quenching of In-X by the addition of Al is consistent with the case of unidentified centers in germanium (References 5,34). These observations may indicate that a selection rule is active on allowed infrared energy levels in silicon. As a speculation (Reference 34) one might consider a doped silicon crystal

to be a macroscopic quantum system in which some levels are forbidden because other levels are occupied. An interesting presentation of the Group IIIA related acceptor energies (B through Tl, including all X-levels) is given in Figure 20. The relative spacings are reminiscent of an energy level diagram for an atomic nucleus.

Another noteworthy result of our CZ Si:(In, Al) study is the lack of agreement between experiments as to the dopants observed and their concentrations. For instance, photoluminescence does not observe any dopant shallower than indium, due to exciton tunneling. Even though the Al concentration was a factor of ten higher in the CZ Si:(In, Al) samples with nearly identical In concentrations compared to the FZ Si:(In, Al) samples studied previously (Reference 7), Al was still not observed indicating that tunneling saturation has not been achieved. In contrast, absorption, photoconductivity and Hall measurements all show the presence of aluminum in the samples. However, the absorption and Hall experiments disagree on the concentration of aluminum present as seen in Table 8. Absorption and Hall measurements also disagree on the amount of boron and aluminum x-level present. One possibility is that the Hall concentration curve cannot resolve the close Al-X and B activation energies and thereby produces a higher B concentration while eliminating Al-X. Whatever the cause, we have experienced difficulties in analyzing these highly doped CZ Si:(In, Al) samples. These same difficulties were not experienced with the more lightly doped FZ Si:(In, Al) samples.

Some other interesting features of the CZ Si:(In, Al) data should also be reviewed at this point. For instance, the presence of only four out of ten excited state lines in absorption and photoconductivity spectra indicates a high total concentration of dopants in the CZ Si:(In, Al) samples. Also, in the photoconductivity spectra the indium and aluminum excited state lines remain as negative peaks up to higher sample temperatures than in singly doped samples. It appears that the presence of a shallower level suppresses the photo-thermal ionization of a deeper impurity. And, one last feature to recall is that the temperature dependence of the Al-X excited states is the same as for simple acceptor excited states. This information should be helpful in analyzing various models for the aluminum x-level.

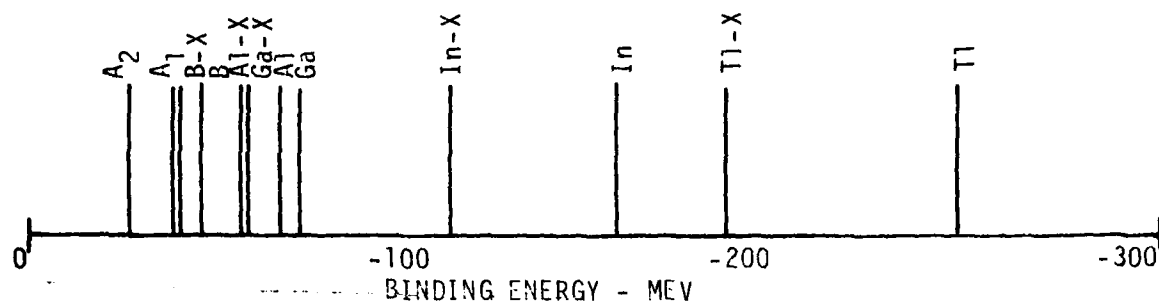


Figure 20. Spectral Representation Of Group IIIA Acceptor Energies In Silicon

TABLE 8

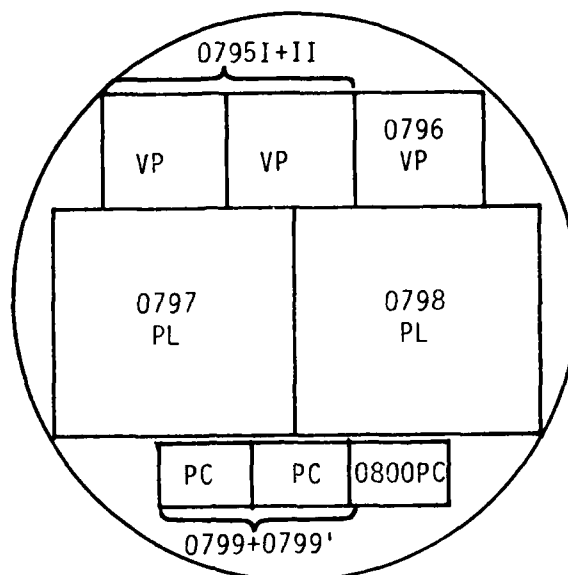
IMPURITY CONCENTRATIONS DETERMINED BY ABSORPTION AND HALL MEASUREMENTS FOR AS-GROWN CZ Si:(In, Al) SAMPLES

Impurity or Dopant	Hall Effect (cm ⁻³)		IR Absorption (cm ⁻³)	
	0795-I	0795-II	0797	0798
In	5.8×10^{16}	2.4×10^{16}	6.0×10^{16}	3.6×10^{16}
In-X	--	--	$<10^{15}$	$<10^{15}$
Al	7.2×10^{16}	2.9×10^{16}	1.8×10^{16}	7.0×10^{15}
Al-X	--	--	5.4×10^{14}	5.3×10^{14}
B	5.9×10^{15}	1.2×10^{15}	6.0×10^{14}	6.8×10^{14}
Donors	2.3×10^{15}	8.8×10^{14}	--	--

Based on our experiences with the present CZ Si:(In, Al) samples and the previous FZ Si:(In, Al) samples, we feel that there are several research areas worth pursuing. One research area would be to resolve the difficulties encountered in determining dopant concentrations for multiply doped samples. This may be achieved by choosing two dopants, possibly In and Ga, which are measurable by an independent means, i.e. neutron activation analysis (NAA). The absorption and Hall concentration measurements could then be calibrated against the NAA concentration results. In addition, a set of Si:(In, Ga) calibration samples could be generated by varying the compensation level through the use of neutron transmutation doping. This sample set would demonstrate the effects of compensation level on Hall and absorption concentration measurements. Another future research area would be to determine at what concentration ratio the deeper acceptor dominates the photoluminescence spectrum through the exciton tunneling mechanism. Between the FZ and CZ Si:(In, Al) samples, the aluminum concentration was varied an order of magnitude while the indium concentration was kept nearly constant. In both cases no photoluminescence features were observed for the shallower aluminum acceptor. Therefore, the next step would be to lower the indium concentration while keeping the aluminum concentration constant. Then one could determine at which concentration ratio the aluminum related features begin to appear in photoluminescence data. A third area for further research would be the influence of aluminum on oxygen precipitation as a means of internal gettering. In low temperature processes aluminum may enhance or degrade gettering. Hence, a study of oxygen precipitation in silicon doped with C, O, and Al should be investigated. Overall, the multiply doped Si:(In, Al) samples have proven to be a very interesting system to study from the materials characterization point of view.

APPENDIX A

SAMPLE LISTING AND WAFER CUTTING DIAGRAM



van der Pauw, VP - 3/8" x 3/8"

Photoluminescence } PL - 1/2" x 1/2"
Absorption

Photoconductivity, PC - 3mm x 6mm

Figure A-1. Sample Listing And Wafer Cutting Diagram

APPENDIX B

CARBON AND OXYGEN LOCAL MODE ABSORPTION
IN PHOTOCONDUCTIVITY

Based on absorption data, carbon and oxygen local mode absorptions in silicon are known to occur at 608 cm^{-1} for substitutional carbon and at 1128 cm^{-1} and 1136 cm^{-1} for interstitial oxygen. Due to the presence of aluminum in the CZ Si:(In, Al) samples, there is a large photoconductive background response in these regions where C and O local mode absorptions occur. Enlarged illustrations of the carbon and oxygen local mode lines in a photoconductivity (PC) spectrum of sample 0800 are seen in Figures B-1 and B-2. These absorption lines are visible in the photoconductive spectrum because the local modes absorb some of the photons that otherwise would have been available to directly excite holes into the valence band. This leads to a decrease in the photoconductive response at the local mode energies relative to nearby continuum photon energies. Hence, negative peaks are observed in the PC spectrum at the local mode positions.

As expected, these negative peaks in PC look very much like their counterparts in absorption spectra. Perhaps these carbon and oxygen peak heights in PC can be calibrated to C and O concentrations as they are in absorption data. At this point there is not enough data to attempt a calibration scheme for photoconductivity. We hope to pursue this point further in the future. The determination of carbon and oxygen concentrations from photoconductivity data could lead to increased sensitivity in the measurement of these impurities.

Another interesting point is that the ratio of the two (1128 cm^{-1} and 1136 cm^{-1}) oxygen peak heights exhibits the same temperature dependence in photoconductivity and absorption. In absorption measurements, the fact that the oxygen lines at 1128 cm^{-1} and 1136 cm^{-1} change their intensity ratio as a function of temperature and can be used as an internal sample temperature calibration has been noted before (References 35,36). In Figure B-3 we present a graph of sample temperature versus the ratio of the $1128\text{ cm}^{-1}/1136\text{ cm}^{-1}$ peak heights based on our absorption and photoconductivity measurements for Cz Si:(In,Al).

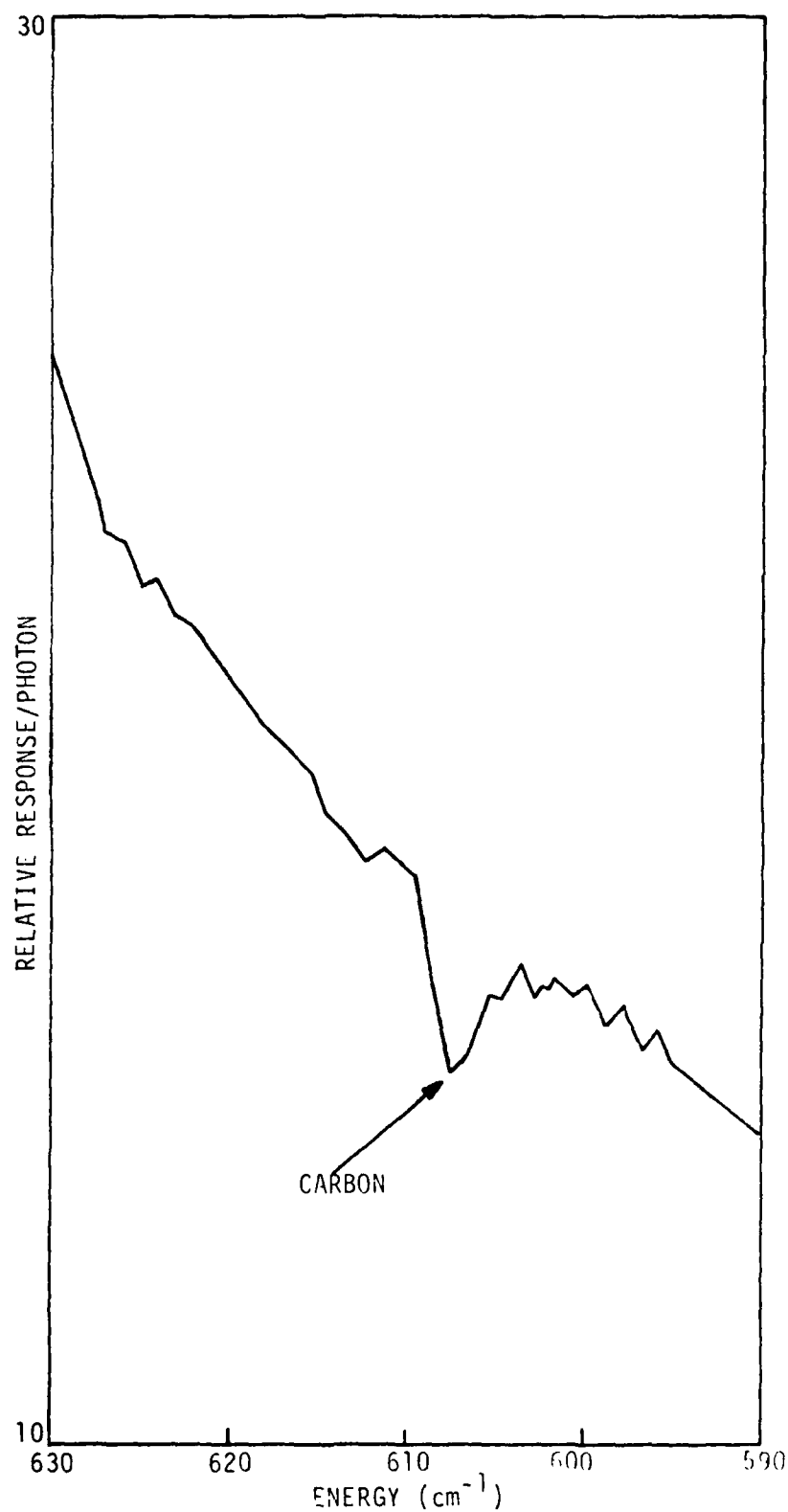


Figure B-1. Carbon Local Mode Absorption Peak In Photoconductivity Spectrum Of CZ Si:(In, Al)

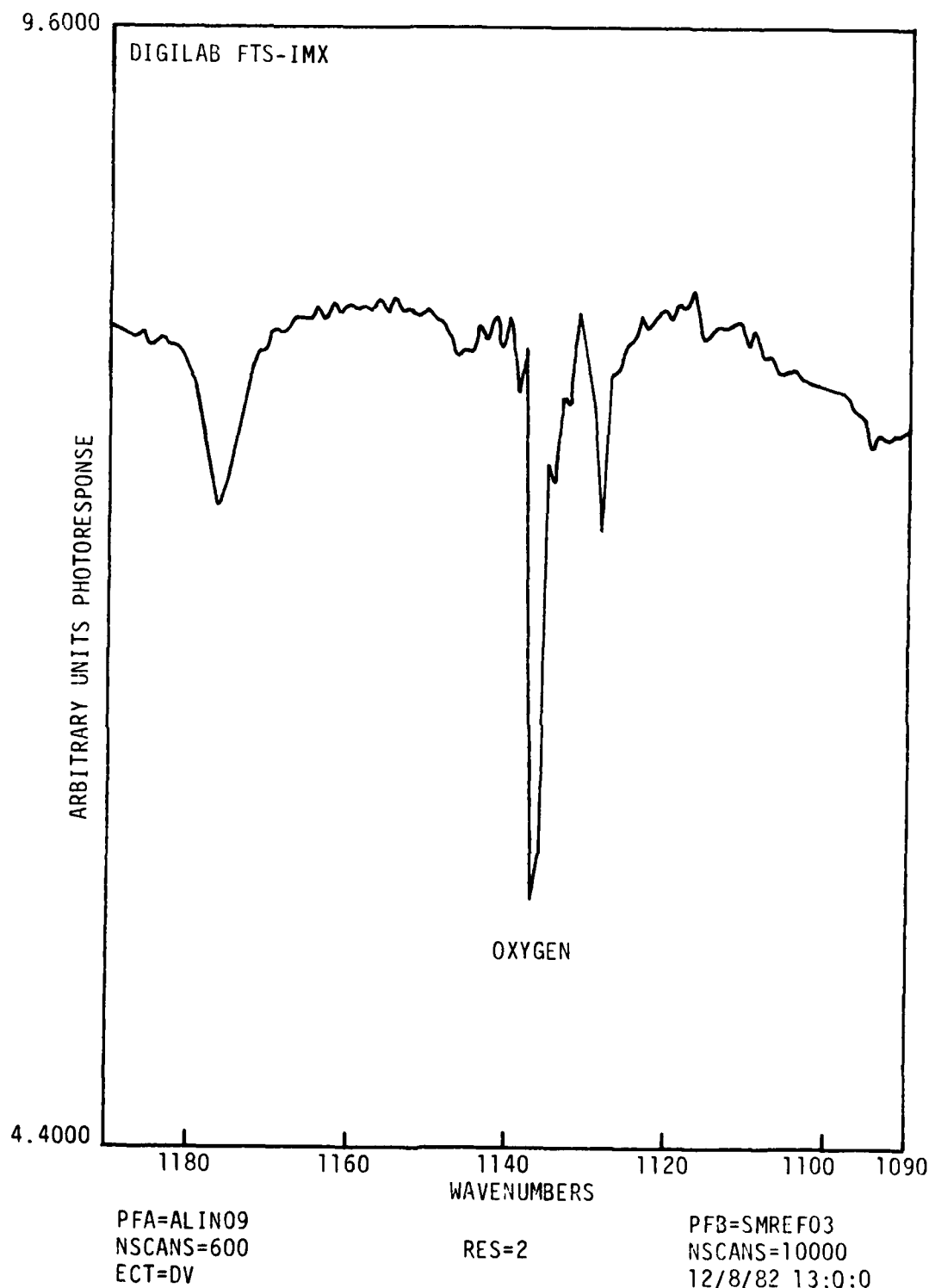


Figure B-2. Oxygen Local Mode Absorption Peaks In Photoconductivity Spectrum Of CZ Si:(In, Al)

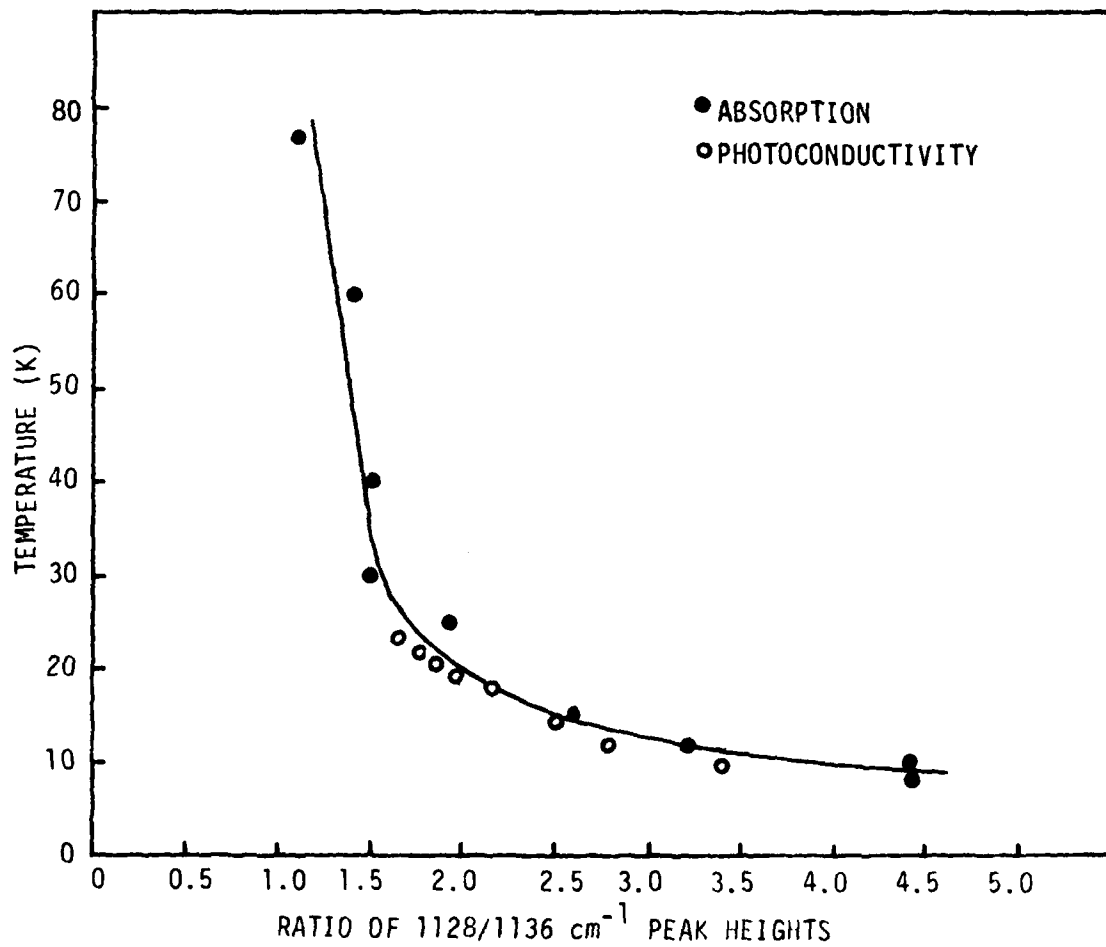


Figure B-3. Sample Temperature vs. Ratio of $1128\text{cm}^{-1}/1136\text{cm}^{-1}$ Oxygen Peak Heights

REFERENCES

1. J. W. Chen and A. G. Milnes, *Ann. Rev. Mater. Sci.* 10, 157 (1980).
2. R. Baron, M. H. Young, J. K. Neeland, and O. J. Marsh, *Appl. Phys. Lett.* 30, 594 (1977).
3. R. Baron, J. P. Baukus, S. B. Allen, T. C. McGill, M. H. Young, H. Kinmura, H. V. Winston, and O. J. Marsh, *Appl. Phys. Lett.* 34, 257 (1979).
4. C. E. Jones, D. Schafer, W. Scott, and R. J. Hager, *J. Appl. Phys.* 52, 5148 (1981).
5. M. C. Ohmer and J. E. Lang, *Appl. Phys. Lett.* 34, 750 (1979).
6. V. A. Panteleev, T. S. Gugina, and V. A. Muravev, *Sov. Phys. Solid State* 20, 324 1978.
7. D. H. Brown, M. C. Ohmer, K. D. Beasley, J. J. Rome, G. J. Brown, and D. W. Fischer, *J. Appl. Phys.* 53, 8793 (1982)(AFWAL-TR-83-4145).
8. J. Baukus and T. C. McGill, "Characterization and Analysis of Indium Doped Silicon Extrinsic Detector Material," Final Report for Contract No. DAAK70-77-C-0082, 1980.
9. J. I. Pankove, Optical Processes in Semiconductors, Dover Publications, Inc., New York, 1971.
10. A. Onton, P. Fisher, and A. K. Ramdas, *Phys. Rev.* 163, 686 (1967)
11. D. W. Fischer and J. J. Rome, *Phys. Rev. B* 27, 4826 (1983).
12. J. J. White, *Can. J. Phys.* 45, 2797 (1967).
13. W. Scott, *Appl. Phys. Lett.* 32, 540 (1978).
14. W. Scott and C. E. Jones, *J. Appl. Phys.* 50, 7258 (1979).
15. J. J. Rome, Masters Thesis, Air Force Institute of Technology, November 1982 (AFIT/GEP/PH/82-D-29).
16. D. W. Fischer, unpublished results.
17. G. D. Watkins and W. Beall Fowler, *Phys. Rev. B* 16, 4524 (1977).
18. T. C. Chandler, R. J. Spry, G. J. Brown, J. J. Rome, and R. J. Harris, *Phys. Rev. B* 26, (1982).
19. G. J. Brown, unpublished results.

REFERENCES (Cont'd)

20. SH. M. Kogan and T. M. Lifshits, Phys. Stat. Sol. (a) 39, 11 (1977).
21. C. W. Searle, M. C. Ohmer, and P. M. Hemenger, Solid State Commun, 44, 1597 (1982).
22. J. Weber, R. Sauer, and P. Wagner, J. Lumin. 24/25, 929, (1981).
23. P. M. Hemenger, Rev. Sci. Instrum. 44, 698, (1973).
24. B. C. Dobbs, P. M. Hemenger, and S. R. Smith, J. Elect. Mat. 6, 705, (1977).
25. F. L. Madarasz, J. E. Lang, and P. M. Hemenger, J. Appl. Phys. 52, 4646 (1981).
26. The temperature dependence of the carrier concentration effective mass for p-type silicon is given by (see Ref. 23):

$$\frac{m_p(T)}{m_0} = \frac{N(T)^{2/3}}{D(T)}$$

$$N(T) = 0.4435870 + aT = bT^2 = cT^3 + dT^4$$

$$D(T) = 1 + eT + fT^2 + gT^3 + hT^4$$

m_0 = electron rest mass

$$a = 0.3609528 \times 10^{-2}$$

$$b = 0.1173515 \times 10^{-3}$$

$$c = 0.1263218 \times 10^{-5}$$

$$d = 0.3025581 \times 10^{-8}$$

$$e = 0.4683382 \times 10^{-2}$$

$$f = 0.2286895 \times 10^{-3}$$

$$g = 0.7469271 \times 10^{-6}$$

$$h = 0.1727481 \times 10^{-8}$$

REFERENCES (Concluded)

27. The functional form used for the Hall scattering factor as a function of temperature was:

$$r(T, ^\circ K) = 0.54 + \frac{1.22 (T/50)}{1.0 + (T/50)^2}$$

J. E. Lang, Private communication.

28. D. K. Schroder, T. T. Braggins, and H. M. Hobgood, J. Appl. Phys. 49, 5256 (1978).
29. T. Peterson, Private Communication.
30. M. W. Jenkins, J. Electrochem. Soc. 124, 757 (1977).
31. D. K. Arch and D. E. Schafer, SPIE, Vol. 285, Infrared Detector Materials, 1981, pg. 175.
32. M. Neuberger and S. J. Welles, Silicon, EPIC Document DS-162, 1969, p. 52.
33. D. H. Brown and S. R. Smith, J. Lumin. 21, 329 (1980).
34. L. Remho, Private Communication.
35. K. Krishnan, Digilab brochure, Note No. 39 (1981).
36. R. C. Newman, Infra-red Studies of Crystal Defects, Taylor and Francis Ltd., London (1973).

REPRODUCED

FILMED

DTIC

